

CHEMISTRY AND DYNAMICS IN PRE-PROTOSTELLAR CORES

JEONG-EUN LEE, NEAL J. EVANS II, AND YANCY L. SHIRLEY

Department of Astronomy, The University of Texas at Austin, Austin, Texas 78712-1083
jelee, nje@astro.as.utexas.edu, yshirley@aoc.nrao.edu

AND

KEN'ICHI TATEMATSU

National Astronomical Observatory of Japan, 2-21-1 Osawa, Mitaka, Tokyo, 181-8588, Japan
k.tatematsu@nao.ac.jp*Draft version April 15, 2018*

ABSTRACT

We have compared molecular line emission to dust continuum emission and modeled molecular lines using Monte Carlo simulations in order to study the depletion of molecules and the ionization fraction in three preprotostellar cores, L1512, L1544, and L1689B. L1512 is much less dense than L1544 and L1689B, which have similar density structures. L1689B has a different environment from those of L1512 and L1544. We used density and temperature profiles, calculated by modeling dust continuum emission in the submillimeter, for modeling molecular line profiles. In addition, we have used molecular line profiles and maps observed in several different molecules toward the three cores. We find a considerable diversity in chemical state among the three cores. The molecules include those sensitive to different timescales of chemical evolution such as CCS, the isotopes of CO and HCO⁺, DCO⁺, and N₂H⁺. The CO molecule is significantly depleted in L1512 and L1544, but not in L1689B. CCS may be in the second enhancement of its abundance in L1512 and L1544 because of the significant depletion of CO molecules. N₂H⁺ might already start to be depleted in L1512, but it traces very well the distribution of dust emission in L1544. On the other hand, L1689B may be so young that N₂H⁺ has not reached its maximum yet. The ionization fraction has been calculated using H¹³CO⁺ and DCO⁺. The result shows that the ionization fraction is similar toward the centers of the three cores. This study suggests that chemical evolution depends on the absolute timescale during which a core stays in a given environment as well as its density structure.

1. INTRODUCTION

Many studies have been done on low mass-star formation in detail, theoretically and observationally, over the past two decades. These studies were possible because many low mass protostellar cores are close, isolated, and geometrically simple. In addition, they evolve slowly, allowing the process to be observed in distinct stages. The information accumulated by those studies now provides the big picture of the evolutionary stages of low-mass star formation. Lada (1987), Myers & Ladd (1993) and André et al. (1993) developed an evolutionary sequence based on the spectral energy distribution (SED) of dust continuum emission through Class 0 to Class III sources, and Adams et al. (1987) supported the evolutionary sequence by modeling the SED theoretically. In addition, several groups (Larson 1969, Penston 1969, Shu 1977, Shu et al. 1987, Foster & Chevalier 1993, Ciolek & Mouschovias 1994, McLaughlin & Pudritz 1997) have developed dynamical evolution models that theoretically predict different structures of density and velocity in protostellar cores, based on differing initial conditions.

In spite of the big picture of low-mass star formation, the initial collapse is poorly understood. The collapse dynamics and the timescale of evolution are crucially dependent on initial conditions. Preprotostellar cores (hereafter PPCs) are believed to be gravitationally bound, but they have no central hydrostatic protostar (Ward-Thompson et al. 1994, 1999). Therefore, PPCs can be considered as

the potential sites of future star formation and give us chances to probe the initial conditions of star formation. The series of papers of Ward-Thompson et al. (1994, 1999, 2000, and 2001) and the paper of André et al. (1996) argued that the density of PPCs is relatively constant in the inner cores and falls off at larger radii. This is very different from the singular isothermal sphere that leads to the “inside-out” collapse (Shu 1977). However, they assumed a uniform temperature in PPCs to calculate density structures. Evans et al. (2001) and Zucconi et al. (2001) show that the temperature of a dust grain decreases toward the centers of PPCs, assuming that dust grains are heated only by the attenuated external radiation field and that the radiation from the core itself is optically thin. Based on their results, Evans et al. (2001) argue that the continuum emission is significantly dependent on the temperature structure as well as the density structure, and they show that Bonnor-Ebert spheres can fit well the submillimeter dust continuum emission in PPCs. In agreement, the recent paper of Ward-Thompson et al. (2002) has shown that the color temperatures of PPCs that are calculated from the 170 and 200 μ m dust emission observed by ISOPHOT decrease toward their centers. As a result of the lower temperature at the center, the density at the center must be more peaked than is the intensity of dust continuum emission. Evans et al. (2001) showed that even a power law could fit the density structure of L1544.

Ciolek & Mouschovias (1994) modeled ambipolar diffu-

sion for the quasi-static evolution of a uniformly magnetized isothermal molecular cloud, finding relatively constant density toward the center. However, there has been debate about the importance of ambipolar diffusion because of differences between inward velocity observed (Tafalla et al. 1998, Williams et al. 1999) and calculated from the magnetic field (Goodman and Heiles 1994, André et al. 1996, Ward-Thompson et al. 1999, Crutcher and Troland 2000, Ward-Thompson et al. 2000). Those differences might be resolved by calculating more accurate density structure and, in turn, the correct temperature structure from the observed data. Ciolek and Basu (2000) showed if the density at the center of a PPC were higher, then their model could explain the observed magnetic field and inward velocity.

In addition to density and temperature distributions, we need to understand the ionization structure because magnetic relaxation by ambipolar diffusion is tightly related to the ionization structure (Rawlings 2000). Ionization fraction can affect the process of gravitational collapse because the coupling between ions and magnetic field plays a key role in preventing free-fall collapse of a dense core and slowing the drift of neutral gas through the magnetic field (ambipolar diffusion). In addition, the gas-phase chemical reactions depend significantly on ionization fraction, and the ionization fraction is highly sensitive to the depletion of molecules because some molecules play a crucial role in destroying ions. The degree of ionization in cold dense cores can be measured by the $[\text{DCO}^+]/[\text{HCO}^+]$ abundance ratio (Watson 1977), which is directly related to the electron density and depletion fraction. Recently, many molecular line observations show evidence for chemical differentiation and the depletion of some molecules such as C^{17}O , C^{18}O , and CCS in dense cores (Lada et al. 1994, Kuiper et al. 1996, Black et al. 1995, McMullin et al. 1994, Benson and Myers 1998, Willacy et al. 1998, Kramer et al. 1999, Ohashi et al. 1999, Caselli et al. 1999, Jessop and Ward-Thompson 2001, Tafalla et al. 2002). They suggested that this trend is due to the substantial depletion of molecules onto dust grain surfaces. In addition, several groups (Bergin and Langer 1997, Aikawa et al. 2001, Caselli et al. 2002, Li et al. 2002) modeled chemical evolution, including gas-dust interaction as well as gas-gas interaction, to show the changing depletions of some molecules and ionization fraction with time or density, and most of them compared their results to real observations. Therefore, both gas phase chemical processes and dust-gas interactions should be considered in studying star formation.

Those theoretical and observational results suggest that the relative distributions of several molecules can be used to probe the timescale of the dynamical evolution of a PPC. However, Rawlings et al. (1992) and Rawlings and Yates (2001) modeled several molecular lines combining self-consistently dynamical, chemical, and radiative transfer models, and showed that the abundance variation and the line profiles are very sensitive to the free parameters in the chemical model. Consequently, we need to use multiple transitions and maps in order to constrain these models.

In this paper, we explore the chemical and dynamical differences in three PPCs (L1512, L1544, and L1689B) comparing molecular depletion and ionization fraction by

simple analysis of integrated intensity and column density and by modeling several molecular line profiles in detail. In this study, we cover a very early-time molecule (CCS), an early-time molecule (CO), a middle-time molecule (HCO^+), and a very late-time molecule (N_2H^+) in chemical evolution. According to the chemical models of Bergin and Langer (1997) and Aikawa et al. (2001) that used an initial density of 10^4 cm^{-3} , the CCS abundance decreases rapidly after a few times 10^5 years since CCS is a polar molecule, and it is easily frozen out onto the surface of dust grains. In addition, CCS is destroyed by HCO^+ or H_3O^+ , whose abundances increase until about 10^6 years. Even though CO is a non-polar molecule, it has very high binding energy (1740 K onto water ice mantle grains, Bergin and Langer 1997). As a result, CO starts to be depleted onto the surface of dust grains after about 10^6 years causing the depletion of HCO^+ in turn. HCO^+ is formed by the interaction between H_3^+ and CO or H_2D^+ and CO. However, N_2 , which is the precursor of N_2H^+ , starts to be abundant much later than other molecules and reaches its maximum around 10^7 years. N_2 has low binding energy (750 K, Aikawa et al. 2001) onto the surface of dust grains, so it is not frozen out from the gas phase easily. In addition, H_3^+ , which is the other precursor of N_2H^+ , increases as CO is depleted. Another cause of the enhancement of N_2H^+ at late times is the decline of the destruction of N_2H^+ by CO, which is significantly depleted at late times.

We observed multiple positions in each core to study the chemical distribution within a core in addition to studying the chemical differences among the three PPCs. The most important aspect of this study is that we start with reasonable physical models calculated from dust analysis. The density and temperature structures found by Evans et al. (2001) are adopted for modeling molecular line profiles.

In section 2, we summarize observational parameters, and section 3 shows the results of observations. In section 4, we analyze column densities of several molecules. Section 5 compares modeled molecular line profiles and observed line profiles. Finally, we discuss our results regarding depletion and ionization in the view of chemical and dynamical evolution in section 6.

2. OBSERVATION

We observed the three pre-protostellar cores in C^{18}O ($J = 2 - 1$ and $J = 3 - 2$), C^{17}O ($J = 2 - 1$), DCO^+ ($J = 3 - 2$), HCO^+ ($J = 3 - 2$), and H^{13}CO^+ ($J = 3 - 2$) with the 10.4 m telescope of the Caltech Submillimeter Observatory (CSO) at Mauna Kea, Hawaii from 1995 to 2002. We used an SIS receiver with an acousto-optic spectrometer (AOS) with a 50 MHz bandwidth and 1024 channels, and the frequency resolution was about 2 to 2.5 channels, 0.13 to 0.16 km s^{-1} at around 220 GHz. The pointing uncertainty was about $4''$ on average. We also observed these cores in H^{13}CO^+ ($J = 1 - 0$), N_2H^+ ($J = 1 - 0$), and CCS ($N_J = 4_3 - 3_2$) with the 45 m telescope of the Nobeyama Radio Observatory in Japan on January 2002. We used the S40, S80, and S100 receivers with an AOS with 40 MHz bandwidth and 2048 channels. The frequency resolution was about 2 channels (about 40 kHz) so that the velocity resolution was about 0.27, 0.14, and 0.13 km s^{-1} at 43, 86, and 100 GHz, respectively. The observed sources are listed in Table 1; the observed lines and the main beam

efficiency (η_{mb}) of each observation are summarized in Table 2. In Table 1, the last column shows the offsets of the dust peaks from the given coordinates; all offsets in figures other than Figure 2 and 3 are relative to the dust peak, assumed to be the center of the core in all modeling.

3. RESULTS

3.1. Spectra

Figure 1 shows the spectra of molecular lines observed toward the centers of the three PPCs. The centers are the positions of the centroid of the dust emission (Shirley et al. 2000). Most of the molecular lines have not been mapped completely but observed through two orthogonal cuts in $\alpha - \delta$, crossing at the centers of dust emission in the cores. We do not see any consistent trend in the intensity of each spectrum from core to core. For example, $C^{18}O$ and $C^{17}O$ lines are the strongest in L1689B, but N_2H^+ and CCS are the strongest in L1544. All the lines except for N_2H^+ and CCS are much weaker in L1512 than in L1689B. The line width (FWHM) of the $C^{18}O$ $J = 2 - 1$ line is about 0.3, 0.5, and 0.6 $km\ s^{-1}$ in L1512, L1544, and L1689B, respectively.

3.2. Maps

Figure 2 shows maps of three PPCs, where the grey scale indicates 850 μm dust continuum intensity and the contours are for integrated intensities of $C^{18}O$ $J = 2 - 1$ and DCO^+ $J = 3 - 2$ lines. We can see that the peaks of dust emission and $C^{18}O$ $J = 2 - 1$ emission are not consistent. In the map for L1512, especially, the centroid of the dust emission coincides with a hole in the $C^{18}O$ $J = 2 - 1$ emission. In contrast, the distribution of DCO^+ $J = 3 - 2$ emission appears to peak toward the center of dust emission in L1544 and L1689B, even though our maps of DCO^+ $J = 3 - 2$ emission are not complete.

4. SIMPLE ANALYSIS

In this section, we use a simple analysis with standard techniques for comparison to similar work done by others, and, in the next section, we will deal with detailed models. We use dust emission as the tracer of column density least affected by chemistry in this section, and we assume that the dust emissivities do not change with radius. If temperature decreases toward the center, the column density calculated from dust emission with the assumption of an isothermal case could be underestimated toward the center. Even though the absolute column density calculated from the dust emission can change with the assumed dust opacity by a factor of 2 or 3, its relative distribution with radius can be traced relatively well by dust emission.

4.1. Integrated Intensities

We can compare the distribution of a molecular component with that of the dust component within a core using the integrated intensity of an optically thin molecular line and the dust continuum intensity observed at a submillimeter wavelength. In the upper panels of Figure 3, we plot the logarithmic integrated intensities of CCS $N_J = 4_3 - 3_2$, $H^{13}CO^+$ $J = 1 - 0$, and N_2H^+ $J = 1 - 0$ lines in order to compare to the 850 μm dust continuum intensity through the cuts with constant declination shown in Figure 2. The dust continuum intensity and the $H^{13}CO^+$

intensity have been shifted upward to compare the shapes of intensity distributions with radius more effectively, and the intensity of dust continuum has been measured into apertures of $20''$, spaced by $20''$ for consistency with the $H^{13}CO^+$ and N_2H^+ observations.

The dust emission of L1512 is about half of that of L1544, and the distribution is not as peaked as that of L1544 and L1689B. L1544 and L1689B have similar dust emission even though it is more peaked in L1544. However, the CCS intensity of L1689B is more similar to that of L1512 rather than to that of L1544, and the CCS intensity of L1544 is about twice those in L1512 and L1689B. The CCS intensity in all the three PPCs is not peaked as much toward the center as the dust emission. However, it has a bump toward the centers of L1512 and L1544 (see §6.1). In L1689B, the bump is not certain because of the low signal-to-noise ratio.

If we check the relative variations of the integrated intensity of the $H^{13}CO^+$ $J = 1 - 0$ line with radius in each core, in L1689B, it is skewed to the west but follows well the dust continuum emission, decreasing at the edge of the core. On the other hand, the distribution of the integrated intensity of the $H^{13}CO^+$ $J = 1 - 0$ line in L1512 is not well matched with dust continuum, and the integrated intensity is even depressed toward the center. We also see the depression of $H^{13}CO^+$ emission at the center of L1544. This depression was predicted by Caselli et al. (2002) in their chemical models, but not observed, probably because their angular resolution ($28''$) was worse than ours ($18''$). We suspect that the optical depth of the $H^{13}CO^+$ $J = 1 - 0$ line in L1544 and L1689B is not negligible. Therefore, the depression in those cores could be partially caused by optical depth. However, L1689B does not show a depression even though it has a density structure similar to L1544 suggesting that depletion is playing a major role in L1544.

The N_2H^+ intensity is well peaked in L1544 and shows almost the same shape as the dust emission. L1689B also shows similar shapes in dust emission and N_2H^+ intensity. However, the N_2H^+ intensity of L1689B is only two thirds of that of L1544, even though these two cores have very similar dust emission and density structures, with central densities of $10^6\ cm^{-3}$. In L1689B, the peak of the intensity of N_2H^+ is shifted from that of the intensity of the dust emission similarly to the intensity of $H^{13}CO^+$. However, the ratio of the intensity of $H^{13}CO^+$ to the intensity of N_2H^+ at the center of L1689B, is greater than that in the other two cores.

In L1512, with a central density of $10^5\ cm^{-3}$, N_2H^+ emission is more extended than the dust, unlike in the other cores. Since the optical depth of the N_2H^+ $J = 1 - 0$ line in L1512 is smaller than in L1544 (Benson et al. 1998), this might indicate the possible presence of depletion at the dust peak.

In the following section, we compare the distributions of CO isotopes to that of dust emission by using molecular hydrogen column densities calculated from them instead of using the intensity distribution because the optical depth effect in the $C^{17}O$ line can be calculated, and the standard abundance of CO is known.

4.2. Column Density

We compare the H₂ column densities calculated from observed molecular line intensities with that calculated from submillimeter continuum emission. This simple analysis assumes that 1) dust continuum emission traces all material along a line of sight in a core, and dust and gas are well mixed, 2) the core is isothermal, and dust and gas are well coupled so that they have same temperature, 3) molecular abundances are constant through the core, and 4) all levels are in LTE. Therefore, the excitation temperatures in all levels are the same as the kinetic temperature and the same as the dust temperature.

4.2.1. The H₂ column density from molecular emission lines

If we assume a line is very optically thin so that absorption can be completely neglected, the equation of radiative transfer is given by

$$\frac{dI_\nu}{ds} = \frac{h\nu_{ul}A_{ul}}{4\pi}n_u, \quad (1)$$

where n_u is the number density of upper level, and A_{ul} is the Einstein coefficient. For the transition $J \rightarrow J-1$ in a linear molecule, the resulting relation between $N(x)$, the column density of molecule x , and the integrated intensity of the line, is

$$N(x) = \frac{3kQe^{E_u/kT_{ex}}}{8\pi^3\nu\mu^2J} \int T_R dv, \quad (2)$$

where $E_u = hBJ(J+1)$, B is the rotational constant, T_{ex} is the excitation temperature above the ground state, μ is the dipole moment, and Q is the partition function. Equation 2 is valid only in the limit that $\tau \rightarrow 0$. For finite optical depth, an optical depth correction can be applied:

$$N_{thick} = N_{thin} \frac{\tau_\nu}{1 - e^{-\tau_\nu}}. \quad (3)$$

In principle, one should also correct for the presence of the cosmic background radiation, T_{cmb} , but for the lines considered here, at $\lambda < 1.4$ mm, the Planck function in temperature units is less than 0.23 K, completely negligible compared to likely values of T_{ex} . The effect on $N(x)$ of neglecting T_{cmb} is less than 5% for $T_{ex} \geq 10$ K and $\tau \leq 1$, typical of the conditions relevant here. These effects are less than any plausible calibration uncertainty.

The rotational constant and the dipole moment of each molecule used for this calculation are listed in Table 3. For the excitation temperature, we used the kinetic temperature of 10 K, a typical value in dark molecular clouds, under the assumption that all lines are thermalized, that is, $T_i = T_{ex} = T_k = 10$ K. If we use 20 K for this calculation, the result is changed only by a factor of 1.2 for the $J = 2-1$ line of C¹⁸O and C¹⁷O.

We calculated the column densities using C¹⁸O $J = 2-1$ and C¹⁷O $J = 2-1$ lines. First, the lines were assumed to be optically thin. However, we can calculate the optical depth of the C¹⁷O $J = 2-1$ line directly by comparing the relative intensities of its 9 hyperfine components (Ladd et al. 1998). The optical depth of the C¹⁷O $J = 2-1$ line was obtained by a fitting method in the program CLASS. The panels in the third row of Figure 1 shows the results of fitting the hyperfine components of the C¹⁷O $J = 2-1$

line in the center of each core. The total optical depths for L1544 and L1689B are not small enough to be ignored (Table 4), even though each individual hyperfine component is optically thin. In order to correct for this optical depth effect, we applied equation (3) to the above calculation for an optically thin line. For the C¹⁷O $J = 2-1$ line, τ_ν is the optical depth of the line center that is calculated by multiplying the relative strength (0.693) of the main group, which has four close components, by the total optical depth. The correction factors at the centers of L1544 and L1689B are about 1.4. Note that we do not use the excitation temperature of C¹⁷O $J = 2-1$ obtained by fitting the hyperfine structure to calculate the column density of C¹⁷O because this method assumes that T_{ex} is constant along the line of sight. Our detailed models (see §5.3.1) shows that this assumption leads to incorrect results. Also we want to use the same method for C¹⁸O and C¹⁷O and compare the results.

Finally, we convert the column density of each molecule into the H₂ column density using the abundance (X) of molecule x ;

$$N(\text{H}_2) = \frac{N(x)}{X(x)} \text{ cm}^{-2}. \quad (4)$$

We used a CO abundance of 2.7×10^{-4} (Lacy et al. 1994), about three times bigger than the abundance used in other studies such as Bacmann et al. (2002) and Jorgensen et al. (2002). The abundance ratios [CO/C¹⁸O] and [C¹⁸O/C¹⁷O] are about 560 (± 25) and 3.2 (± 0.2), respectively (Wilson and Rood, 1994). The abundance of each molecule used in calculating the H₂ column density is listed in Table 3.

4.2.2. The H₂ column density from dust continuum emission

If the emission from dust is optically thin, the observed flux density (S_ν) can be related to the column density of gas by

$$N(\text{H}_2) = \frac{S_\nu}{\mu m_H \kappa_\nu B_\nu(T_d) \Omega}, \quad (5)$$

where μ is the mean molecular weight, m_H is the atomic mass unit, κ_ν is the mass opacity of dust per gram of gas, B_ν is the Planck function, and Ω is the aperture solid angle. $\Omega = (\pi\theta^2)/(4\ln 2)$ for a circular Gaussian aperture.

We use column 5 of the Ossenkopf-Henning dust opacity table (Ossenkopf & Henning 1994), which represents agglomerated dust grains with thin ice mantles, and assume a gas-to-dust mass ratio of 100 to get $\kappa_{850} = 0.018 \text{ cm}^2 \text{ g}^{-1}$. We use the 850 μm data from Shirley et al. (2000) but measure the flux in an aperture of $33''$, the size of main beam in the observations of C¹⁷O. If the dust temperature, T_d is 10 K, the H₂ column density can be calculated from

$$N(\text{H}_2) = 3.36 \times 10^{22} \times S_{850}(\text{Jy}) \text{ cm}^{-2}. \quad (6)$$

If the temperature were 20 K, the calculated $N(\text{H}_2)$ would be lower by a factor of 3.3.

4.2.3. Results

$\text{C}^{18}\text{O } J = 2 - 1$ and $\text{C}^{17}\text{O } J = 2 - 1$ lines have been used to calculate the H_2 column density assuming constant molecular abundances. Basically, we assume the lines are optically thin. If a molecular line is optically thick, then the calculation with equation (2) and (4) underestimates the H_2 column density. As mentioned in the previous section, however, we can calculate the optical depth of the $\text{C}^{17}\text{O } J = 2 - 1$ line by fitting its hyperfine structure. We have corrected the column density of the $\text{C}^{17}\text{O } J = 2 - 1$ line for optical depth in L1544 and L1689B even though the correction is not very big.

The results of fitting the hyperfine components of $\text{C}^{17}\text{O } J = 2 - 1$ show that the total optical depth of this line is about 0.1 in L1512, but it is not negligible at the central positions in L1544 ($\tau \approx 1.0$) and L1689B ($\tau \approx 0.8$). In L1512, the error of the calculated optical depth is very big, because of the low S/N in the weak components. However, the ratio (≈ 4.3) between the strongest component and the second strongest component in L1512 is bigger than that (≈ 3.3) in the two other cores, so the total optical depth would be less than that of L1689B, at least. The abundance of C^{18}O is about 3.2 times greater than that of C^{17}O . Therefore, the optical depth of C^{18}O is about 3.2 greater than the total optical depth of C^{17}O , and the optical depth of $\text{C}^{18}\text{O } J = 2 - 1$ must be considered in calculating column densities. We plot the H_2 column density calculated from the $\text{C}^{17}\text{O } J = 2 - 1$ line in the lower panes of Figure 3, where the optical depth effect has been corrected by equation (3). However, in the figure, we use the H_2 column density calculated from the $\text{C}^{18}\text{O } J = 2 - 1$ line based on the optically thin line approximation without correcting for its optical depth in order to show the significance of the optical depth effect. In fact, C^{17}O has been observed in fewer positions so that we cannot calculate the optical depth of every C^{18}O spectrum.

In the figure, we see significant differences between the H_2 column densities calculated from the $850 \mu\text{m}$ emission and the $\text{C}^{18}\text{O } J = 2 - 1$ line in all three PPCs. At central positions, the H_2 column density calculated from the $\text{C}^{18}\text{O } J = 2 - 1$ line is about 15 times smaller in L1512 and L1544, and 8 times smaller in L1689B than the H_2 column densities calculated from the $S_{850} \mu\text{m}$ emission. However, after correcting for the optical depth of the $\text{C}^{17}\text{O } J = 2 - 1$ line, the difference between the H_2 column densities calculated from S_{850} and from C^{17}O has been reduced. In L1689B, especially, the difference is just a factor of 2 after the correction.

Another interesting thing is that the distribution of C^{17}O in L1544 does not show the central depression observed in Caselli et al. (1999). This is probably due to the larger beam ($33''$) in this observation compared to that ($21''$) of Caselli et al. (1999), similarly to the case of H^{13}CO^+ (see §4.1). This result suggests that inadequate resolution can prevent us from calculating the actual depletion of molecules.

4.3. Conclusions

The integrated intensities and the H_2 column densities calculated from several molecules have been compared with the intensity of $850 \mu\text{m}$ dust emission and the H_2 column densities calculated from the dust emission in our

simple analysis of molecular line observations. The first result of this analysis is that the dust emission is more peaked than the molecular emission. The depression of molecular emission toward the centers is partially caused by the optical depth effect on molecular lines. We could see this effect comparing the column densities calculated from $\text{C}^{17}\text{O } J = 2 - 1$ (marginally optically thin and corrected by τ) and $\text{C}^{18}\text{O } J = 2 - 1$ (optically thick but not corrected by τ) lines. The correction for the optical depth effect by the $\text{C}^{17}\text{O } J = 2 - 1$ line removes some of the difference between the H_2 column densities calculated from the $\text{C}^{18}\text{O } J = 2 - 1$ line and dust emission. The remaining considerable discrepancy would be caused by the depletion of CO molecules. This result shows that we can overestimate the depletion of a molecule if we use an optically thick line without correcting for the optical depth. Jorgensen et al. (2002) have compared the H_2 column densities calculated from the 1.3 mm dust continuum and the $\text{C}^{17}\text{O } 1-0$ line and found similar depletion factors of CO to ours in L1544 and L1689B. We will explore the depletion in detail through modeling molecular line profiles using the Monte Carlo method in the next section. We emphasize that the amount of the discrepancy varies from core to core. After the correction for the optical depth effect, the H_2 column density calculated from the $\text{C}^{17}\text{O } J = 2 - 1$ line is 11 in L1512, 9 in L1544, and 2 in L1689B times smaller than the H_2 column density calculated from dust emission (Table 5).

The simple method used in this analysis clearly reveals evidence for depletion, but it has several limitations for quantitative analysis. First, the beam size of each line observation is not the same. If we had mapped these cores completely in each line, then we would have been able to convolve the maps using the same beam size. Second, the variations of the excitation temperature and the abundance of a molecule along the line of sight are not included in this simple analysis. In addition, the absolute H_2 column density calculated from dust emission may be uncertain by a factor of 2 to 3 because of the uncertainty of dust opacity. Due to these limitations, we have to model molecular lines and compare them to the observed lines in order to study depletion more in detail.

5. DETAILED MODELS

5.1. Method

We used the Monte Carlo (hereafter MC) method to calculate the radiative transfer of molecular lines (Bernes 1979, Choi et al. 1995). The MC code for this work has been developed by Choi et al. (1995). The MC code generates model photons at a random position, in a random direction, and at a random frequency with proper random number distributions. These photons go through a one-dimensional spherically symmetric molecular cloud adjusting the level populations of molecules. The MC code calculates the excitation by the model photons and uses statistical equilibrium to adjust each level population until the criteria of convergence are satisfied. The MC method is more powerful than the LVG method because it can deal with arbitrary distributions of systematic velocity, density, kinetic temperature, microturbulence, and abundance self-consistently. Therefore, we can combine reasonable physical models from analysis of dust emission with chemical

models to produce molecular line simulations, and the depletion of molecules with radius can be tested.

For the MC simulation, we needed collision rates at lower gas temperatures than are usually available, so we extrapolated linearly to 5 K the collision rates for CO (Flower and Launay 1985), which we used for C¹⁸O and C¹⁷O. Similarly, we extrapolated the downward collision rates for HCO⁺ (Flower 1999) to use for H¹³CO⁺ and DCO⁺. Upward rates were calculated for detailed balance for each isotope. The size of each core is fixed at 0.15 pc, and microturbulent velocity is assumed constant through each modeled core.

Once the MC code calculates each level population, we simulate specific molecular line profiles using the virtual telescope (VT) simulation to compare the modeled profiles with observed molecular line profiles. We can simulate a molecule with multiple transitions and multiple positions simultaneously in a specific core with the parameters such as beam sizes and main beam efficiencies that we used in the actual observations. The remaining lack of realism is caused by geometric differences between a 1-dimensional simulation and the actual core. As seen in Figure 2, the three cores are not perfectly spherically symmetric, but instead they are elongated. In order to compare simulated line profiles with real observations, we averaged the lines that have been observed at the same distance from the centers, e.g., the lines in the off-positions of $\pm 30''$ in α and δ . However, some lines have not been averaged in all four directions because the observation did not cover all parts. We need to map cores fully and use a 2-dimensional code to do more accurate comparisons.

We model the transitions of four molecules, C¹⁸O ($J = 2 - 1$ and $J = 3 - 2$), DCO⁺ ($J = 3 - 2$), H¹³CO⁺ ($J = 1 - 0$ and $J = 3 - 2$), and HCO⁺ ($J = 3 - 2$). If the gas and dust of a core are well mixed and well coupled, we can apply the distributions of density and temperature of the dust to the gas. However, for a density lower than about 10^4 cm^{-3} , the gas temperature is not coupled well with the dust temperature. The excitation temperatures of the lines that have high critical density such as DCO⁺ and H¹³CO⁺ are mainly dependent on density so that the inner, denser region mainly contributes to the intensities of those molecular lines, and the outer, less dense region does not change our results much. However, we should in principle correct for the difference between gas and dust temperatures in the outer, less dense parts of cores, especially for the molecular lines such as C¹⁸O lines that have low critical density. We leave this correction for a future work.

5.2. Physical Models

We use two different types of physical models: Bonnor-Ebert spheres (Bonnor 1956, Ebert 1955); and Plummer-like models (Whitworth & Ward-Thompson 2001). Both these models allow an initial density distribution that is nearly constant for small radii, but approaches a power law at large radii. The Bonnor-Ebert sphere provides a good fit to the dust continuum emission of the three PPCs that we are modeling (Evans et al. 2001). The Plummer-like model can fit the dust continuum data for L1544 (Whitworth & Ward-Thompson 2001). It has the advantage that it provides a simple solution for the density and velocity field during a free-fall collapse from the initial state,

thereby providing a velocity field, which we need for modeling some of our lines. The initial Plummer-like radial density profile (Whitworth and Ward-Thompson 2001) is

$$\rho(r, t = 0) = \rho_{flat} \left[\frac{R_{flat}}{(R_{flat}^2 + r^2)^{1/2}} \right]^\eta. \quad (7)$$

Even though this model is very simple, in that it assumes a pressure-free collapse, it may be able to explain the later phase of the evolution of PPCs. Li et al. (2002) show that the evolution of a core driven by ambipolar diffusion becomes closer to the evolution of a non-magnetic, free-falling core at higher density.

We use the Bonnor-Ebert sphere model that best fit the dust emission (Evans et al. 2001), and we assume a purely microturbulent velocity field, except for the HCO⁺ $J = 3 - 2$ lines in L1544 and L1689B and the H¹³CO⁺ lines in L1544. Because those line profiles show deep self-absorption features indicative of systematic radial velocities, we use a Plummer-like model for them. To constrain the various parameters in the Plummer-like model, we modeled the dust emission, as was done by Evans et al. (2001). The resulting values that fit best the data for both L1689B and L1544 are as follows: $\eta = 3$, the initial ρ_{flat} ($t=0$) of $5 \times 10^5 \text{ cm}^{-3}$, and R_{flat} of 2800 AU. Whitworth and Ward-Thompson found a steeper density structure ($\eta = 4$) and a bigger R_{flat} (5350 AU) because they used an isothermal sphere for their model. When the temperature decline toward the center is included, a smaller R_{flat} is needed. The evolutionary timescale that fits the dust emission well is half the timescale at which the central point-mass is formed (the start of the Class 0 stage). The maximum velocity in this model is about 0.08 km/s, which is consistent with the results of Tafalla et al. (1998) and Williams et al. (1999) in L1544. The resulting density structure is compared to that of the best fitting Bonnor-Ebert sphere in Figure 4a; they are very similar. Likewise, the resulting dust temperature structure is very similar (Figure 4b). The velocity field from the Plummer-like model is shown in Figure 4c.

While the density and temperature structure of the best-fitting Plummer-like model is very similar to that of the best fitting Bonnor-Ebert sphere, the former does contain a systematic velocity field. To check whether that field affected the results for lines modeled with the Bonnor-Ebert sphere, we modeled all other lines using the Plummer-like model. The velocity structure does not affect the line profiles of C¹⁸O, DCO⁺, and H¹³CO⁺; the two models have given the same results.

5.3. Results of Models

The main purpose of this modeling is to find how much a specific molecule is depleted, and how the depletion is distributed with radius by simulating molecular line profiles at multiple positions within a core and by comparing the simulated line profiles with observed line profiles. We tried several functional forms, such as exponential, power laws, Plummer-like, and step functions, for the distribution of a molecular abundance. In addition, we applied the results of Li et al.'s dynamical and chemical model (2002) to our modeling, but their model has too high a systematic velocity to fit the observed molecular line profiles. However, the group is improving their chemical and

dynamical models while communicating with us. Figure 5 and Table 6 shows the comparison between results of different functional forms of depletion with radius in the $C^{18}O$ 2–1 line simulations. We used integrated temperatures to calculate χ^2 in each model. Among those distributions, a step functional distribution fits best the observed line profiles with radius. This seems reasonable because the results of chemical models show a sharp decrease in abundance with density or time. Here, we mainly show the results of the modeling with the abundance distribution of a step function that has three free parameters: the undepleted abundance of a molecule (X_0), the fractional depletion ($f_D = X/X_0$), and the radius inside which a molecule is depleted (r_D). Each can be different in different species. Therefore, the total depletion of a molecule is dependent on the combination of f_D and r_D . We emphasize that the derived depletion factor from this modeling has an uncertainty of about a factor of 3 because of the uncertainty of the density structure calculated from the dust analysis.

We compared the distributions of observed and modeled integrated temperatures with radius to find the best fits. Figure 6.a shows the distribution of the reduced χ^2 of the models in the $C^{18}O$ 2–1 and 3–2 lines of L1512 in the space of f_D and r_D . The depletion radius is well constrained around 0.075 pc, but the fractional depletion is constrained only to be greater than about 25. This trend occurs in every molecule that is significantly depleted, so we consider f_D to be the lower limit of the depletion factor. In other words, the data are consistent with complete depletion inside some r_D . However, the distribution of χ^2 constrains only the upper limit of the depletion radius in $H^{13}CO^+$ and DCO^+ of L1689B and in DCO^+ of L1544, which show small r_D and f_D (see Table 8 and Table 9). For example, the χ^2 in $H^{13}CO^+$ of L1689B changes within a factor of about 2 (from 3 to 7) in all range of f_D within $r_D < 0.011$ (Figure 6.b). As we mentioned above, the density structure has uncertainty of a factor of about 3, so the calculated depletion in this model could have the same uncertainty.

5.3.1. $C^{18}O$ $J = 2 - 1$ and $J = 3 - 2$

The best fits of $C^{18}O$ $J = 2 - 1$ and $J = 3 - 2$ line profiles in the three cores are shown in Figure 7. The parameters of the best fit models are summarized in Table 7. We used the standard $C^{18}O$ abundance of 4.82×10^{-7} for the undepleted abundance (X_0) for all cores, which was used to calculate the column density of H_2 (§ 4.2.1). According to the results, CO molecules are depleted within 0.075 pc (about 110'') by a factor of 25 in L1512, so CO is depleted everywhere in our $C^{18}O$ map. In the case of L1544, the depletion factor is 25 within 0.045 pc (about 70''). $C^{18}O$ $J = 2 - 1$ and $J = 3 - 2$ line profiles simulated simultaneously at different positions from the center fit the observed line profiles well in L1512 and L1544. On the other hand, we could not find a model to fit well all the observed line profiles from the center to the off-position of 90'' in L1689B. The antenna temperatures of observed $J = 2 - 1$ and $J = 3 - 2$ lines are almost the same or increase outward from the center in L1689B, even though the outermost lines are not well sampled. This might indicate that the large molecular cloud surround-

ing this source (Loren 1989) contributes to the observed $C^{18}O$ lines. We tested a core that has a warm envelope surrounding an inner, denser core. The core has the same density and temperature structures inside 0.15 pc as those calculated from dust emission, and a constant density and temperature of 10^3 cm^{-3} and 50 K from 0.15 to 0.6 pc, which are based on the ^{13}CO observations (Loren 1989). The temperature of 50 K is the upper limit in the ρ Oph molecular complex. The modeled line profiles are shown in Figure 7c, which fit better the observed line profiles than those in the previous model that does not have a warm envelope. In this model, the abundance distribution is the same as the previous one. In order to avoid confusion by the envelope, we need to use a more rare isotope or higher J transition to trace the high density core. Even though L1512 and L1544 are believed to be well isolated, they might also be surrounded by bigger clouds. The modeled results, however, fit well the observed $C^{18}O$ $J = 2 - 1$ to the off-position of 90''. The influence of bigger structures in L1512 and L1544 does not seem significant compared to L1689B.

Jessop and Ward-Thompson (2001) modeled the $C^{18}O$ $J=2-1$ and $J=3-2$ lines of L1689B using a density structure with the same central density (ρ_{flat}) and the same R_{flat} as calculated by André et al. (1996) and a constant temperature. After comparing to observations they argued that the flat distribution of $C^{18}O$ is caused by the significant (about 95%) depletion of CO. They pointed out that the gas temperature must be above 14 K to have better agreement with observations. However, they compared the model to the observation within 32'', which cannot give a good constraint on the outer envelope. In addition, the lower density and higher temperature at the inner region than those assumed in this study make the transitions optically thinner than the actual lines, so the depletion factor to fit the observations could be overestimated. We modeled $C^{18}O$ lines using our density structure and a constant temperature of 14 K. The best-fit model has $r_D \sim 0.035$ and $f_D \sim 10$, which are bigger than our best-fit model, where the temperature structure is calculated from the analysis of dust emission. The modeled $C^{18}O$ $J=2-1$ lines within 60'' are stronger than the observed lines. However, the line at 90'' is still weaker than the observed line even though it is stronger than that in our best-fit model without a warm envelope.

5.3.2. $H^{13}CO^+$ $J = 1 - 0$ and $J = 3 - 2$

Except for the $C^{18}O$ lines, X_0 is not fixed in modeling molecular lines, but it can be easily decided by the outermost line profile. The results of the best models in $H^{13}CO^+$ $J = 1 - 0$ and $J = 3 - 2$ are shown in Figure 8 and Table 8. We have observed the $H^{13}CO^+$ $J = 1 - 0$ line with a 20'' grid out to the distance of 60'' from the center with an 18'' beam. The $J = 3 - 2$ line has been observed with 30'' spacing with a 26'' beam. In L1512, the $H^{13}CO^+$ $J = 3 - 2$ line, whose critical density is about 10^6 cm^{-3} , was not detected, so we simulated only the $J = 1 - 0$ line. The depletion factor in L1512 is 25 within 0.021 pc (38''). In L1689B, the best-fit model of $J = 1 - 0$ line also fits $J = 3 - 2$ line very well. The depletion factor and radius in L1689B are much smaller than those in L1512. However, the undepleted abundance of $H^{13}CO^+$ in L1512 is

1.4 times bigger than in L1689B.

The observed H^{13}CO^+ $J = 1 - 0$ line, whose critical density is about 10^5 cm^{-3} , shows a blue skewed profile in L1544. Contracting cores show stronger blue peaks and self-absorption dips in optically thick lines (Myers et al. 1996). Evidence of inward motion in L1544 has been observed by Tafalla et al. (1998) and Williams et al. (1999). Therefore, we used the best-fit Plummer-like model in the simulation of the H^{13}CO^+ $J = 1 - 0$ line. In L1544, models fit well the shapes of the observed H^{13}CO^+ $J = 1 - 0$ line profiles, but the modeled $J = 3 - 2$ line is *stronger* than the observed line by a factor of 2. The rms noise of this line is about 0.015 K (5σ detection), and the baseline is poor, so the discrepancy may not be very significant. There are several possibilities. If there is molecular gas surrounding L1544, this less dense gas would increase the $J = 1 - 0$ line more than the $J = 3 - 2$ line. Therefore, our models would overestimate the abundance of the inner, denser core to fit the $J = 1 - 0$ line. As a result, the modeled $J = 3 - 2$ line can be stronger than the observed line. Another possible explanation is that the depletion fraction increases toward the denser, inner region. Since the $J = 3 - 2$ line traces denser gas than the $J = 1 - 0$ line, the $J = 3 - 2$ line in our models where we used a step function of the abundance would be stronger than the observed line if H^{13}CO^+ is depleted more at the center. The uncertainties in the observed line or in the density and temperature structures could explain the difference between the modeled and observed lines.

5.3.3. DCO^+ $J = 3 - 2$

The modeling of DCO^+ $J = 3 - 2$ does not constrain free parameters well because the observations in the line do not cover positions far from the center. The results are shown in Figure 9 and in Table 9. In L1512, only the center position was observed, so we just used a constant abundance to fit the line profile. The abundance of DCO^+ that fits the line profile well is 2.8×10^{-10} . However, the line profiles of two positions in L1544 and three positions in L1689B were compared with the results of models. The factor and the radius of the depletion of DCO^+ molecule are much smaller than those of CO molecules calculated by simulating C^{18}O $J = 2 - 1$ and $J = 3 - 2$ lines. This result is consistent with the results of the chemical model of Caselli et al. (2002). The radius of the depletion is less ($20''$) than the beam size ($35''$) in L1689B and similar to the beam size in L1544.

5.3.4. HCO^+ $J = 3 - 2$

Infall asymmetry in PPCs has been observed (Tafalla et al. 1998, Lee et al. 1999, Gregersen and Evans 2000) in optically thick lines. If the gas of the outermost envelope of a core that has inward motion has sufficient optical depth and has a lower excitation temperature than the gas of the inner envelope in a given molecular line, the molecular line shows infall asymmetry, in which the intensity ratio of blue peak to red peak increases with time (Gregersen et al. 1997). We model one of the optically thick lines, HCO^+ $J = 3 - 2$ in the three PPCs and compare the results with the observational results of Gregersen and Evans (2000). In order to model an HCO^+ $J = 3 - 2$ line that has infall asymmetry, we used the best-fit Plummer-like

model. Figure 10 shows the difference in MC modeling of the HCO^+ $J = 3 - 2$ line for two different physical models: Bonnor-Ebert sphere and Plummer-like model. The latter includes an infall velocity structure and produces a blue asymmetry. The HCO^+ $J = 3 - 2$ line in L1512 does not show a self-absorption dip and asymmetric profile so that we model the line in L1512 using the best-fit Bonnor-Ebert sphere.

The results of modeling HCO^+ $J = 3 - 2$ in the three PPCs are shown in Figure 11, and in Table 10. Because L1512 has only one spectrum at the position $30''$ away from the center, we used a constant abundance of HCO^+ for this core. The abundance of the best fit is about 1×10^{-9} . In L1544, the intensity of the HCO^+ $J = 3 - 2$ line at $30''$ is half that at the center, unlike the H^{13}CO^+ 1-0 line, whose intensity is almost flat to $40''$. As a result, an exponential abundance distribution as well as a step function also fits well the line profiles. In L1689B, the HCO^+ $J = 3 - 2$ line has a stronger red-peak asymmetry at the center and $15''$ away, but it has a stronger blue-peak asymmetry at $30''$ and $45''$. This complication of line profiles causes difficulty in fitting the exact line profiles in this core. Therefore, we tried to fit the integrated temperatures of the lines with radius. The exponential function of the abundance shows similar results to the step function. In order to test the functional form of the abundance, we need a more extended map. The interesting result is that the HCO^+ $J = 3 - 2$ line of L1689B has a similar strength to that of L1544, unlike H^{13}CO^+ 1-0, which is stronger in L1689B than in L1544. This might be due to the fact that L1689B is embedded in a larger molecular cloud that causes more absorption of the HCO^+ 3-2 line.

On the whole, the abundance of HCO^+ in this result is very small compared to the abundance that is expected from H^{13}CO^+ and the typical ratio of C and ^{13}C in the local interstellar medium of about 77 (Wilson and Rood 1994). However, our results show the abundance ratio of HCO^+ and H^{13}CO^+ is approximately from 3 to 15 in the three PPCs. (We do not think that the ratio in L1512 is correct because we used only one spectrum in each line to calculate the abundance.) In addition, the depletion factors and the depletion radii calculated from the HCO^+ line are different from those calculated from the H^{13}CO^+ lines. These differences and the low abundance ratio may result from the gas components outside the cores that we modeled in this study because the HCO^+ line can trace less dense gas than H^{13}CO^+ . As a result, the HCO^+ line can be absorbed by the surrounding material significantly, but the H^{13}CO^+ line may be not absorbed as much as the HCO^+ line. In our models, we limited the size of every core to 0.15 pc so that our models cannot account for the gas outside the core. Then, we would have underestimated the abundance trying to fit a line that has been weakened by the absorption by the surrounding gas component. However, this explanation is just one possibility. We cannot ignore the uncertainties of many other parameters, so we leave this as future work.

6. DISCUSSION

6.1. Depletion

We concluded that CO is significantly depleted in L1512 and L1544. It is difficult to estimate the depletion of CO

in L1689B because of the gas surrounding this core and the optical depths of the lines used, but the depletion appears to be much less. The HCO^+ molecule is depleted in L1512 and L1544, but we do not see significant depletion of this molecule in L1689B, based on modeling the H^{13}CO^+ $J = 1 - 0$ line. The optical depth and possible surrounding material also affect the calculation of the depletion of HCO^+ in L1544. DCO^+ is not significantly depleted in any of the PPCs. This result is consistent with results in many other starless cores where the distribution of DCO^+ fits well the distribution of dust continuum (Myers 2002, personal communication). However, we need to use better resolution to do a more precise study because the calculated depletion radius is not bigger than the actual beam size ($35''$). Caselli et al. (2002) show that the depletion radius of DCO^+ is about 3000 AU in L1544.

The analysis of the integrated intensity shows that the earliest-time molecule CCS is not peaked toward the centers of any of the PPCs, unlike the dust emission. Thus, CCS is depleted significantly in all three. As we saw, however, the CCS intensity in L1544 is twice stronger than that in L1689B even though the dust emission of L1689B and L1544 is similar. This result suggests that the depletion of CCS is connected to the depletion of CO. Li et al. (2002) modeled chemical abundance changes in PPCs using a dynamical model with a magnetic field, which drives the ambipolar diffusion, and they got a relatively high abundance of CCS. They indicated that this abundance could result from the interplay between significant depletion of CO molecules and late-time hydrocarbon chemistry. Ruffle et al. (1997, 1999) also showed the same result in their models of the time-dependence of several molecules. According to their models, the abundance of CCH and CCS have later secondary maxima only when the freeze-out timescale is long compared to the chemical timescale or the collapse timescale. CCS increases quickly to the first maximum of its abundance in time and is depleted very early as the density increases because CCS is destroyed by increasing HCO^+ or H_3O^+ , and this polar molecule can be tightly bound in grain mantles. However, in the region where CO molecules are depleted significantly, the C^+ ion reacts more with molecules that are not oxygen-bearing species so that the precursors of CCS such as CCH increase again. This results in a second increase of the CCS abundance. The trend has not shown up in the models of Bergin & Langer (1997) and Aikawa et al. (2001) because the models used dense initial conditions in which a core evolves very quickly dynamically, and CCS did not show the second maxima. We think that the CCS molecule is possibly in the second enhancement in the late stage of chemical evolution resulting from the significant depletion of CO in L1512 and L1544. The integrated intensity of the CCS line shows bumps in the center regions of L1512 and L1544 (Figure 3). If CCS is depleted with time without the second enhancement, we should see holes rather than bumps. The other possible explanation of the enhancement of CCS is mixing of some atomic carbon from a translucent envelope into the core (van Dishoeck 2002, personal communication).

According to the comparison between the intensity of N_2H^+ lines and the dust emission intensity, this molecule is possibly depleted in L1512, but not in L1544 and L1689B,

where its intensity follows well the dust emission intensity. N_2H^+ is known as a very late-time molecule, but Bergin et al (2002) have shown that N_2H^+ is depleted in a cold dark cloud, B68. The weak intensity of N_2H^+ line in L1689B, compared to in L1544, might indicate that this molecule has not yet reached its maximum because of less abundant precursors (N_2 and H_3^+) but a more abundant destroyer (CO).

Bergin and Langer (1997) modeled chemical evolution in PPCs including gas-grain interactions as well as gas-phase reactions and compared two kinds of grain mantle properties: a weakly bound CO mantle and tightly bound H_2O mantle. Their results show that sulfur-bearing molecules such as CS and SO are very sensitive to density and depleted seriously as the density of a core increases, regardless of the properties of dust grains. On the other hand, CO and HCO^+ molecules are depleted in the model with H_2O grain mantles but remain in gas phase in the model with CO grain mantles. In contrast, NH_3 and N_2H^+ do not show depletion in any model because of the low binding energy of N_2 to H_2O and CO mantles. Therefore, the comparison of the results of their chemical models to our results indicates that the dust grains in the three PPCs have tightly bound H_2O mantles. In addition, Aikawa et al. (2001) predicted the abundance distributions of molecules by numerical chemical models simply by applying a constant delay factor to a Larson-Penston model and considering different sets of adsorption energies, and they compared their results with the observed molecular abundances in L1544. According to their results, CCS and CO molecules are depleted, but N_2H^+ and NH_3 molecules are more abundant in more slowly collapsing cores at the density peak.

To summarize our results on depletion, CCS, CO, and HCO^+ are significantly depleted in L1512 and in L1544. On the other hand, the depletion of DCO^+ in the two cores is not significant. N_2H^+ is not depleted in L1544, but it is possibly depleted in L1512. In contrast, only CCS is significantly depleted in L1689B. It is hard for us to estimate the depletion of CO in L1689B because of the optical depth effect and the material surrounding the cores.

6.2. Ionization

The coupling between ions and the magnetic field is crucial in regulating star formation rates if cores are magnetically subcritical. The timescale of ambipolar diffusion depends on the ionization fraction ($t_{\text{AD}} \approx 2.5 \times 10^{13} x(e)$, Shu et al. 1987). In addition, the gas-phase chemical reactions are also dependent on the ionization fraction. Therefore, calculating the ionization fraction accurately is significant for understanding the chemistry as well as the timescale for ambipolar diffusion. However, it is not easy to calculate the ionization fraction in protostellar cores because it depends on the depletions of molecules as well as density structures and cosmic-ray ionization rate.

We used equation (16) in Caselli (2002) to calculate the ionization fractions:

$$x(e) = \frac{2.7 \times 10^{-8}}{[\text{DCO}^+]/[\text{HCO}^+]} - 1.9 \times 10^{-7} \left[\frac{1}{f_{\text{D}}} + \frac{x(\text{O})/f'_{\text{D}}}{10^{-4}} \right], \quad (8)$$

where f_D is the depletion factor of CO, $x(O)$ is the abundance of atomic oxygen (1.5×10^{-4} , Caselli et al. 1998), f'_D is the depletion factor of O, and $[DCO^+]/[HCO^+]$ is the abundance ratio of two molecules, which can be calculated by comparing the column densities of DCO^+ and $H^{13}CO^+$ and using $77 (\pm 7)$ for the $^{12}C/^{13}C$ ratio (Wilson & Rood 1994). Caselli et al. (1998) and Caselli (2002) derived this equation assuming that (i) the main source of HCO^+ is the reaction between H_3^+ and CO, (ii) the deuterium fractionation is due to the reaction between H_3^+ and HD, and (iii) molecular ions are destroyed mainly by electrons and neutral species such as CO and O. In fact, Caselli et al. (2002) have showed that N_2H^+ and N_2D^+ are better tracers of ionization fraction because HCO^+ and DCO^+ are possibly depleted in the central region. However, we do not have N_2D^+ data, so we use DCO^+ and HCO^+ , which can give correct information in the region with $r > 3000$ AU.

We calculate, for each line of sight, the average $x(e)$ along the line of sight. This approach is not completely self-consistent because the method is only valid for homogeneous clouds. We use our model to simulate observation with the same beam size. The column density of each molecule has been calculated from the simulated line based on the assumption of an optical thin line. Figure 12 shows the ionization fraction with radius in the three PPCs.

There are some caveats in this calculation. First, we could not assess the depletion factor of CO in L1689B correctly because of the optical depth problem and the possible material surrounding the core (§ 5.2.1). Second, the model of $H^{13}CO^+$ lines in L1544 does not match the observations very well so that the calculated column density from the simulated $H^{13}CO^+$ $J = 3 - 2$ has more uncertainty. Third, since we do not have enough observed data to assess the depletion radius of DCO^+ in L1512, the column density of DCO^+ is uncertain in this core too. In addition to the caveats related to models, the equation that we used to calculate ionization fraction includes the abundance and the depletion fraction of O that are not well known. We supposed that the depletion of atomic oxygen might be proportional to the depletion factors of other molecules. We used f'_D of 3, 2, and 1 for L1512, L1544, and L1689B, respectively.

In spite of these caveats, the three cores have similar average ionization fractions (about 5×10^{-7}) along the line of sight toward the centers. These results are similar to the ionization fractions calculated in other protostellar cores (Caselli et al. 1998) but much bigger than the result (about 10^{-9} at the center) of Caselli et al. (2002). Caselli et al. (1998) have used the integrated temperatures of the actual line profiles, but Caselli et al. (2002) have used the results of their “L1544 best-fit” chemical model, which takes into account the cloud density structure, molecular freeze out, and the recombination of molecular ions on grain surfaces, in order to infer the electron fraction as a function of cloud radius. Our data do not rule out still smaller values of $x(e)$ at small radii. The ionization fraction in L1512 and L1544 decreases toward the center, which trend has been shown in Caselli et al. (2002) and Caselli (2002). In contrast, in L1689B, it increases toward the center. As a result, the ionization fraction of L1689B around 0.06 pc is smaller than those of L1512 and L1544

by a factor of 10.

6.3. Timescales

The timescale of ambipolar diffusion ($t_{AD} \approx 2.5 \times 10^{13} x(e)$, Shu et al. 1987) calculated from the above ionization fraction toward the centers is about 1.25×10^7 years. This timescale applies to cores that are magnetically subcritical. This ambipolar timescale represents the duration of contraction from the present stage to the stage of Class 0. These are much bigger than the free fall timescale ($\approx 10^6$ years). However, $x(e)$ could be much smaller at the center. Even though these three cores have similar ambipolar diffusion timescale toward the centers, our results suggest that they have different chemical status from each other.

L1512 seems to have evolved chemically more than L1544 showing that CCS, CO, HCO^+ , and possibly N_2H^+ are depleted. Caselli (2002) modeled a core that is less dense and less centrally concentrated than L1544 to show the chemistry in an early stage in the dynamical evolution. According to their result, molecules in the model core are not significantly depleted. The model core is similar to L1512 in density structure, but surprisingly, L1512 shows a bigger depletion radius of CO than L1544. In addition, N_2H^+ at the center of L1512 might start to be depleted. This result could result from the slower contraction of L1512 than L1544 so that L1512 could have a longer time to evolve chemically. Another possibility is a more efficient molecular freeze out in L1512 because the dust grains in this object are smaller than in the other two cores, so that the depletion timescale in L1512 is shorter (van Dishoeck et al. 1993; Caselli et al., in prep.). This could be possible because L1512 is less dense than the other two cores and has not have enough time for grain coagulation (Evans et al. 2001).

On the other hand, L1689B has not evolved much chemically even though the density structure is very similar to L1544 so that it is in a later stage of dynamical evolution than is L1512. This tells us that the chemical evolution is not a simple function of density, unlike the results of other chemical models. According to this result, we should not ignore the possibility that L1689B could be magnetically supercritical, and the core has evolved faster than the other two sources dynamically so that L1689B has not had enough time to evolve chemically. The broader lines in L1689B (Figure 1 and § 3.1) indicate more active kinematics than the other two sources. The total masses of L1544 and L1689B are similar according to the dust modeling. Therefore, L1689B has to have a weaker magnetic field or a smaller ionization fraction in order to be magnetically supercritical. Crutcher & Troland (2000) measured the magnetic field along the line of sight in L1544 ($B_{LOS} \approx 11 \mu G$) by using the Zeeman effect of the OH lines. There is no specific measurement of magnetic fields in L1689B. However, Troland et al. (1996) measured a OH Zeeman effect in the ρ Oph cloud indicating $B < 10 \mu G$. In addition, our calculation shows the ionization fraction in L1689B is smaller than in the other two cores in the outer part, where the calculation is more credible. The other possibility of the faster dynamical evolution of L1689B than L1544 is a larger external pressure (Galli et al. 2002) because L1689B is in the ρ Oph complex (see §5.3.1).

Based on our results, we suggest that the stage of dynamical evolution of a core cannot be simply probed by its chemical status because the chemical evolution depends on the size of dust grains or the absolute timescale, during which the core has been in a given environment, as well as its density structure that shows the relative stage of dynamical evolution. We summarize the dynamical and chemical evolutionary stages of each core in Table 11.

7. SUMMARY

The summary of our results is as follows:

- 1) The difference between the column densities inferred from dust emission and the emission of a given molecular line can partially result from the optical depth of the line. However, the depletion of a molecule must explain the remaining difference. In L1689B, the main cause of the difference between the dust emission and the CO emission is the optical depth in the lines. However, in L1512, the depletion of CO is the major source of the difference between the dust emission and the CO emission.
- 2) In our Monte Carlo simulation of molecular lines, a step function with depletion in the inner region produces the best fit to the abundance variation of a molecule in PPCs.
- 3) The CO and HCO⁺ molecules are depleted significantly in L1512 and L1544, but not in L1689B. The gas around L1689B makes it difficult to calculate the actual depletion of CO.
- 4) The depletion of DCO⁺ is not substantial in the three PPCs.
- 5) The CCS molecule is substantially depleted in the three PPCs. However, CCS might be in the second enhancement in L1512 and L1544 because of the significant depletion of CO.
- 6) The distribution of the integrated intensity of N₂H⁺ J = 1–0 suggests the possible depletion of N₂H⁺ in L1512. On the other hand, N₂H⁺ follows dust emission very well in L1544. In L1689B, N₂H⁺ has not had enough time to reach its maximum.
- 7) The velocity structures calculated by a simple dynamical model that uses a Plummer-like density profile and a free-fall collapse model can produce the asymmetry of HCO⁺ J = 3–2 lines in L1544 and L1689B. However, the abundance calculated by modeling the lines is much smaller than what is expected from modeling H¹³CO⁺. The surrounding gas could possibly account for the low HCO⁺ abundance of the models.

8) The ionization fraction is similar toward the centers of the three cores even though L1512 is less centrally condensed than L1544 and L1689B. However, L1512 has a bigger depletion radius of CO than L1544 and possible depletion of N₂H⁺ at the center. In contrast, L1689B does not show the maturity in chemical evolution compared to the other two cores. This difference suggests that the chemical evolution depends on the size of dust grains or the absolute timescale during which a core stays in a given environment as well as the density structure of the core that shows the relative dynamical evolutionary stage.

9) The evolved density structure and the young chemistry of L1689B suggest that this core is possibly experiencing a free-fall collapse rather than ambipolar diffusion. As a result, L1689B evolves dynamically too fast to evolve chemically. This would be possible if the magnetic field in L1689B is weak enough, or the external pressure is big enough to make L1689B magnetically supercritical.

8. ACKNOWLEDGMENTS

We are grateful to Paola Caselli, the referee of this paper for helpful comments. We thank the staff of the Caltech Submillimeter Observatory and the Nobeyama Radio Observatory for assistance in using 10.4 m and 45 m telescopes. We also thank E. van Dishoeck, P. Myers, and J. Rawlings for their useful comments. We are very grateful to Z.-Y. Li and V.I. Shematovich for providing the data from their models. We thank State of the Texas and the NSF (Grant AST-9988230) for support. J.-E. Lee thanks the Rotary Foundation for support through an Ambassadorial Scholarship.

REFERENCES

- Aikawa, Y., Ohashi, N., Inutsuka, S.-I., Herbst, E. & Takakuwa, S. 2001, *ApJ*, 552, 639
- Adams, F.C., Lada, C.J., & Shu, F.H. 1987, *ApJ*, 312, 788
- André, P., Ward-Thompson, D., & Barsony, M. 1993, *ApJ*, 406, 122
- André, P., Ward-Thompson, D., & Motte, F., 1996, *A&A*, 314, 625
- Bacmann, A., Lefloch, B., Ceccarelli, C., Castets, A., Steinacker, J., & Loinard, L., 2002, *A&A*, 389, L6
- Bergin, E.A. & Langer, W.D., 1997, *ApJ*, 486, 316
- Bergin, E.A., Alves, J., Huard, T.L., & Lada, C.J. 2002, *ApJ*, 570, L101
- Benson, P.J., Caselli, P., & Myers, P., 1998, 506, 743
- Blake, G.A., Sandell, G. Van Dishoeck, E.F., Groesbeck, T.D., Mundy, L.G., & Aspin, C., 1995, *ApJ*, 441, 689
- Bonnor, W.B. 1956, *MNRAS*, 116, 351
- Caselli, P., Walmsley, C. M., Tafalla, M., & Herbst, E. 1998, *ApJ*, 499, 234
- Caselli, P., Walmsley, C.M., Tafalla, M., & Myers, P.C. 1999, *ApJ*, 523, L165
- Caselli, P., Walmsley, D.M., Zucconi, A., Tafalla, M., Dore, L., & Myers, P.C., 2002, *ApJ*, 565, 331a
- Caselli, P., Walmsley, D.M., Zucconi, A., Tafalla, M., Dore, L., & Myers, P.C., 2002, *ApJ*, 565, 344b
- Caselli, P., 2002, *astro-ph/0204127*
- Ciolek, G.E. & Mouschovias, T.C., 1994, *ApJ*, 425, 142
- Crutcher, R.M. & Troland, T.H., 2000, *ApJ*, 537, L139
- Ebert, R. 1955, *Z. Astrophys.*, 37, 217
- Evans, N.J.II, Rawlings, J.M.C., Shirley, Y., & Mundy, L.G. 2001, *ApJ*, 557, 193
- Flower, D.R., & Launay, J.M, 1985, *MNRAS*, 214, 271
- Flower, D.R., 1999, *MNRAS*, 305, 651
- Foster, P.N., & Chevalier, R.A., 1993, *ApJ*, 416, 303
- Galli, D., Walmsley, M., & Goncalves, J., 2002, *astro-ph/0208416*
- Goldsmith, P.F., 2001, *ApJ*, 557, 736
- Gregersen, E.M., Evans, N.J.II., Zhou, S., & Choi, M., 1997, *ApJ*, 484, 256
- Gregersen, E.M., Evans, N.J.II., 2000, *ApJ*, 538, 260
- Jessop, N.E. & Ward-Thompson, D., 2001, *MNRAS*, 323, 1025
- Jorgensen, J.K., Schoier, F.L., & van Dishoeck, E.F., 2002, *A&A*, 389, 908
- Kramer, C., Alves, J., Lada, C.J., Sievers, A., Ungerechts, H., & Walmsley, C.M., 1999, *A&A*, 342, 257
- Kuiper, T.B.H., Langer, W.D., & Velusamy, T., 1996, *ApJ*, 468, 761
- Lada, C.J., Lada, E.A., Clemens, D.P., & Bally J. 1994, *ApJ*, 429, 694
- Ladd, E.F., Fuller, G.A., & Deane, J.R., 1998, *ApJ*, 495, 871
- Lacy, J.H., Knacke, R., Geballe, T.R., & Tokunaga, A.T., 1994, *ApJ*, 428, L69
- Larson, R.B., 1969, *MNRAS*, 145, 271
- Lee, C.W., Myers, P.C., & Tafalla, M., 1999, *ApJ*, 526, 788
- Li, Z.-Y., Shematovich, V.I., Wiebe, D.S., & Shustov, B.M., 2002, *ApJ*, 569, 792
- Loren, R.B., 1989, *ApJ*, 338, 902
- McMullin, J.P., & Mundy, L.G., 1994, *ApJ*, 424, 222

- McLaughlin, D.E., & Pudritz, R.E., 1997, *ApJ*, 476, 750
 Myers, P.C. & Ladd, E.F., 1993, *ApJ*, 413, L47
 Myers, P.C., Mardones, D., Tafalla, M., Williams, J.P., & Wilner, D.J. 1996, *ApJ*, 465, L133
 Ohashi, N., Lee, S.W., Wilner, D.J., & Hayashi, M., 1999, *ApJ*, 518, L41
 Ossenkopf V. & Henning Th., 1994, *A&A*, 291, 943
 Penston, M.V., 1969, *MNRAS*, 144, 425
 Ruffle, D.P., Hartquist, T.W., Taylor, S.D., & Williams, D.A., 1997, *MNRAS*, 291, 235
 Ruffle, D.P., Hartquist, T.W., Caselli, P., Rawlings, J.M.C. & Williams, D.A., 1999, *Astrophysics and Space Science*, 262, 177
 Rawlings, J.M.C., Hartquist, T.W., Menten, K.M., & Williams, D.A., 1992, *MNRAS*, 255, 471
 Rawlings, J.M.C., 2000, *IAU symposium*, vol. 197, 15
 Rawlings, J.M.C. & Yates, J.A., 2001, *MNRAS*, 326, 1423
 Shirley, Y.L., Evans, N.J.II, Rawlings, J.M.C. & Gregersen, E.M. 2000, *ApJS*, 131, 249
 Shu, F.H. 1977, *ApJ*, 214, 488
 Shu, F.H., Adams, F. C., & Lizano, S. 1987, *ARAA*, 25, 23
 Suzuki, H., Yamamoto, S., Ohishi, M., Kaifu, N., Ishikawa, S., Hirahara, Y., & Takano, S., 1992, *ApJ*, 392, 551
 Tafalla, M., Mardones, D., Myers, P.C., Caselli, P., Bachiller, R., & Benson, P.J., 1998, *ApJ*, 504, 900
 Tafalla, M., Myers, P.C., Caselli, P., Walmsley, C.M., & Comito, C., 2002, *ApJ*, 568, 815
 Troland, T.H., Crutcher, R.M., Goodman, A.A., Heiles, C., Kazes, I., & Myers, P.C., 1996, *ApJ*, 471, 302
 van Dishoek, E.F., Blake, G.A., Draine, B.T., & Lunine, J.I, 1993, in *Protostars and Planets III*, Levy E.H. & Lunine J.I. (eds.). Tucson: University of Arizona Press, p. 163
 Ward-Thompson, D., Scott, P.E., & André, P., 1994, *MNRAS*, 268, 276
 Ward-Thompson, D., Motte, F., & André, P., 1999, *MNRAS*, 305, 143
 Ward-Thompson, D., Kirk, J.M., Crutcher, R.M., Greaves, J.S., Holland, W.S., & André, P., 2000, *ApJ*, 537, L135
 Ward-Thompson, D., André, P., & Kirk, J.M., 2002, *MNRAS*, 329, 257
 Watson, W.D. 1977, *CNO Isotopes in Astrophysics*, ed. J. Audouze, Reidel Publ. (Dordrecht)
 Whitworth, A.P. & Ward-Thompson, D., 2001, *ApJ*, 547, 317
 Willacy, K., Langer, W.D., & Velusamy, T., 1998, *ApJ*, 507, L171
 Williams, J.P., Myers, P.C., Wilner, D.J., & di Francesco, J., 1999, *ApJ*, 513, L61
 Wilson, T.L. & Rood, R.T., 1944, *ARAA*, 32, 191
 Zhou, S. Evans, N.J.II, Kompe, C., & Walmsley, C. M. 1993, *ApJ*, 404, 232
 Zucconi, A., Walmsley, C.M., & Galli, D., 2001, *A&A*, 376, 650

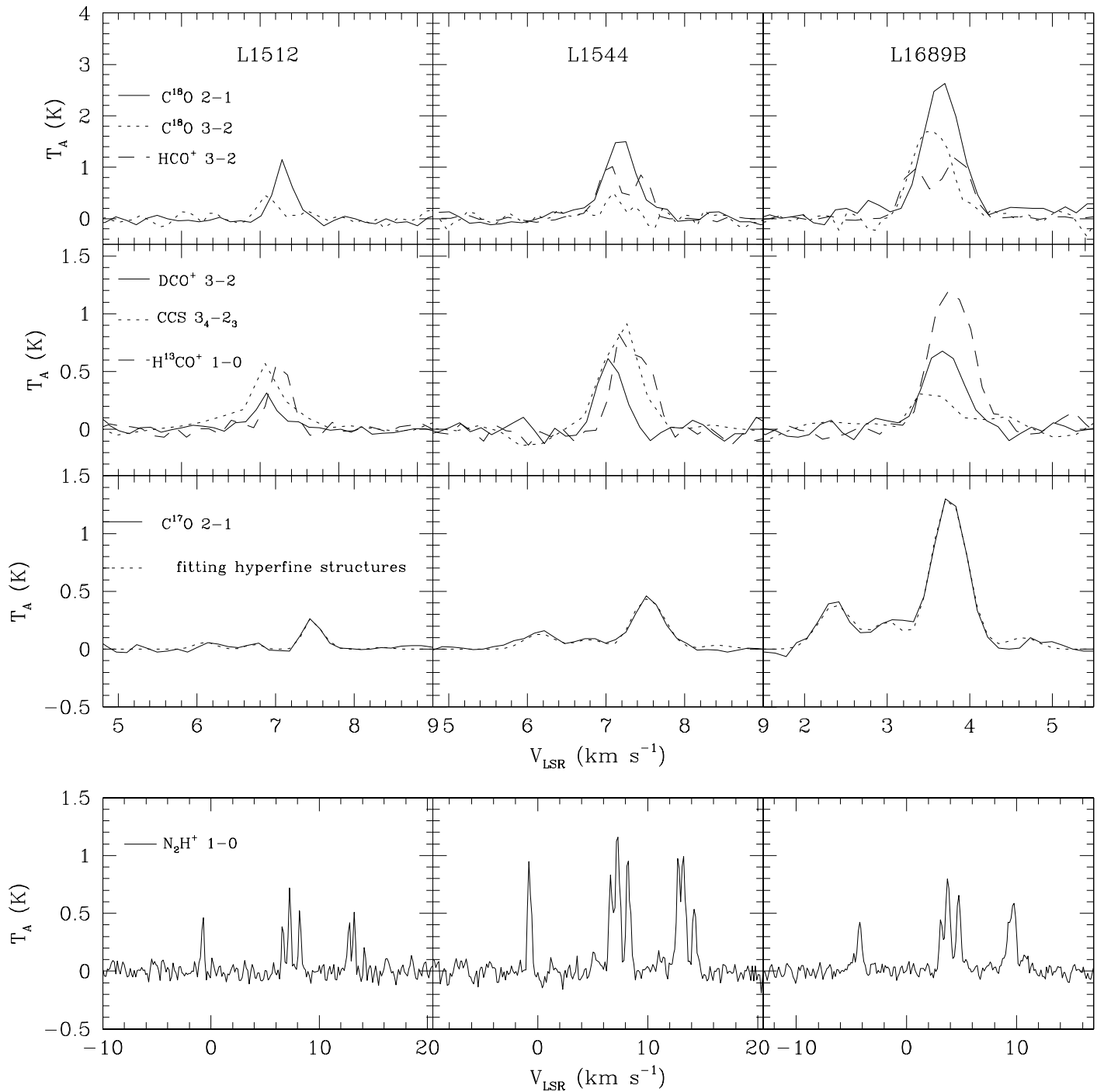


FIG. 1.— The observed spectra toward the dust peaks of three PPCs. The dotted line in the boxes of the third row shows the results of fitting the hyperfine structure of C^{17}O $J = 2 - 1$ line profiles using solutions in CLASS.

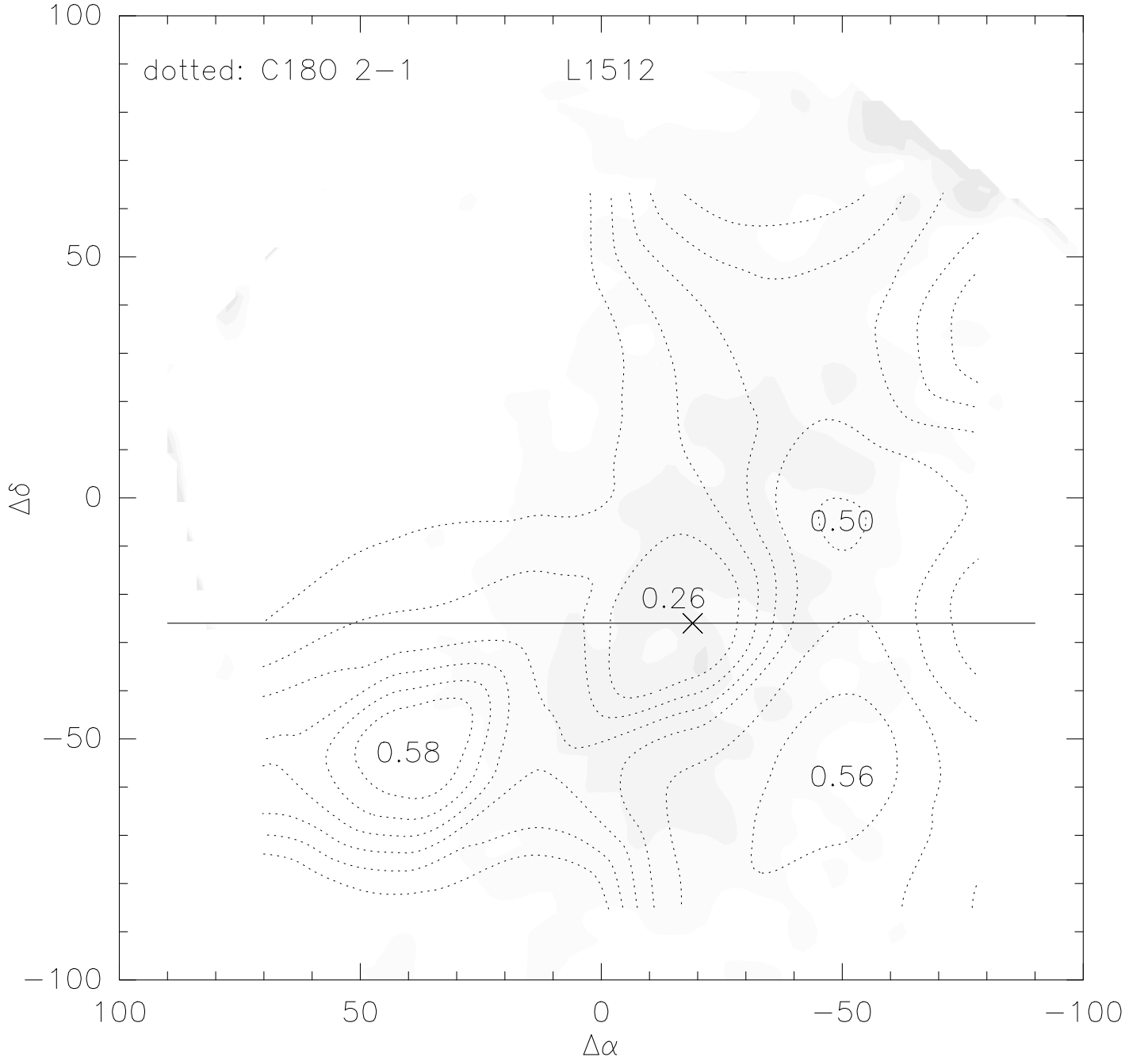


FIG. 2.A.— These maps show the distributions of $850\ \mu\text{m}$ dust continuum intensity (grey scale, Shirley et al. 2000) and integrated intensities of $\text{C}^{18}\text{O}\ J = 2 - 1$ line (dotted contour scale) and $\text{DCO}^+\ J = 3 - 2$ line (solid contour scale). The $(0,0)$ position is the reference position in Table 1. The contour levels are from $3\ \sigma$ intensity to peak intensity by $1\ \sigma$ intensity. For L1512, we put integrated intensity values in several points to distinct a hole and peaks. Cross marks indicate the central peak positions of $850\ \mu\text{m}$ dust continuum emission, and horizontal lines show the cuts that we compare integrated intensities of CCS , H^{13}CO^+ , and N_2H^+ transitions or the column densities calculated from $\text{C}^{18}\text{O}\ J = 2 - 1$ and $\text{C}^{17}\text{O}\ J = 2 - 1$ transitions.

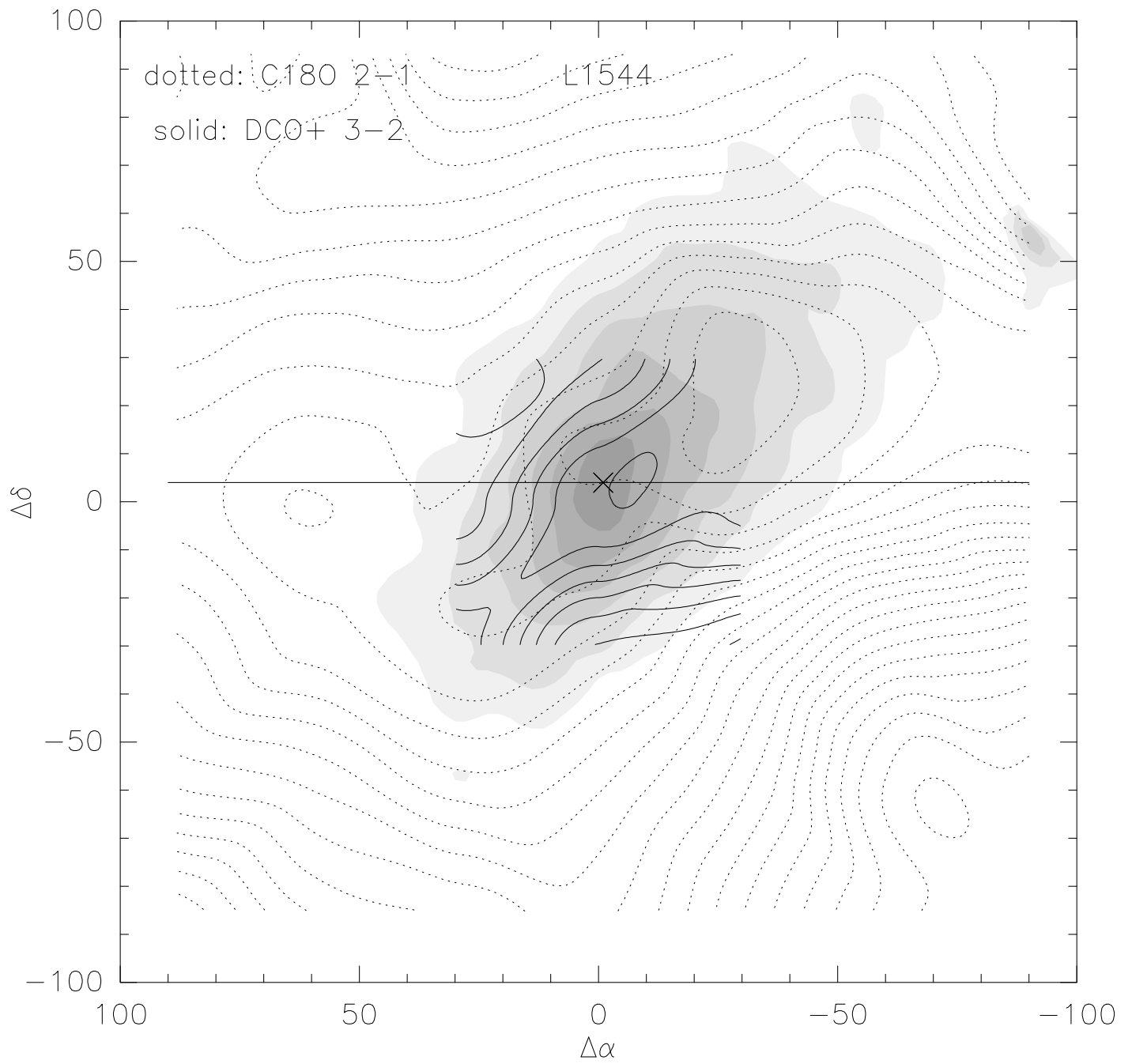


FIG. 2.B.—

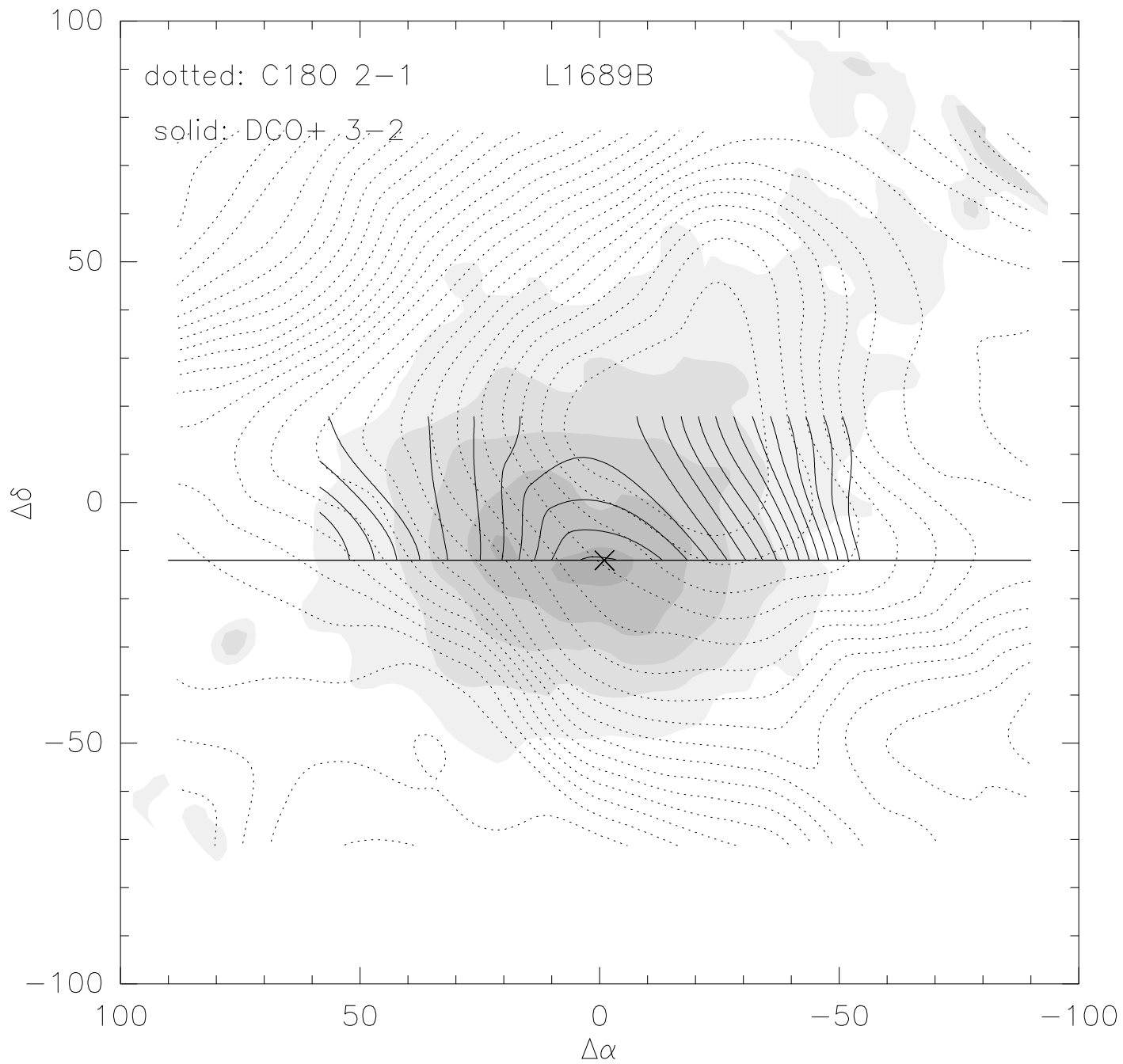


FIG. 2.c.—

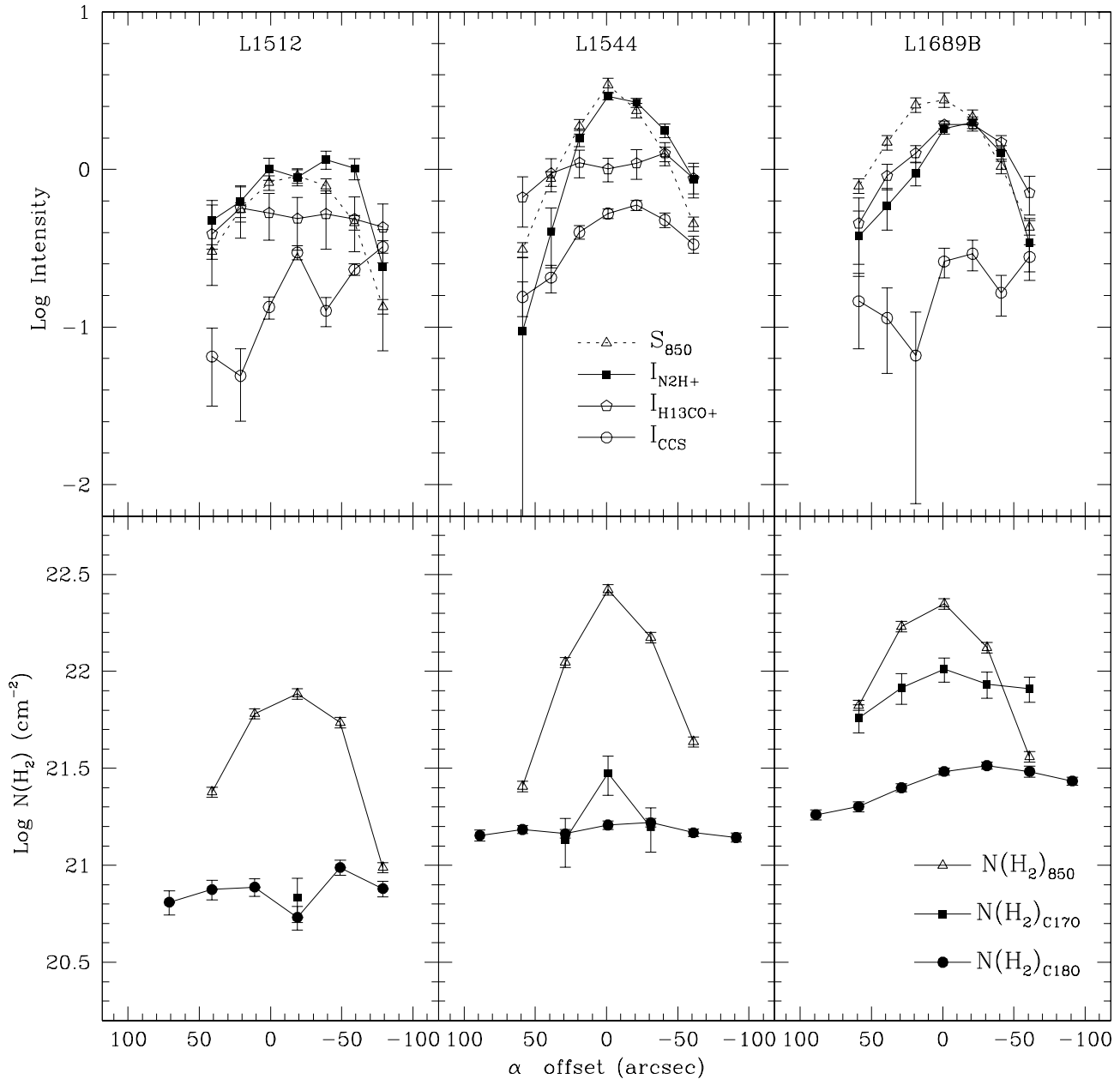


FIG. 3.— These plots in upper panels compare the integrated intensities of CCS $N_J = 4_3 - 3_2$, $H^{13}CO^+ J = 1 - 0$, and $N_2H^+ J = 1 - 0$ lines with S_{850} through the cuts marked in Figure 2. Here, S_{850} is shifted by 0.9, and $I_{H^{13}CO^+}$ is shifted by 0.4 in the logarithmic scale. These plots in lower panels compare the column densities of hydrogen molecules calculated from the $850 \mu m$ dust continuum emission, $C^{18}O J = 2 - 1$ line (without the correction of τ), and $C^{17}O J = 2 - 1$ line (with correction of τ) through the cuts marked in Figure 2. The errors in molecular intensities only account for the rms noises of spectra so that the error bars show the minimum errors. In $N(H_2)$ derived from $C^{17}O$ of L1544 and L1689B, the error in fitting the hyperfine structure is also included.

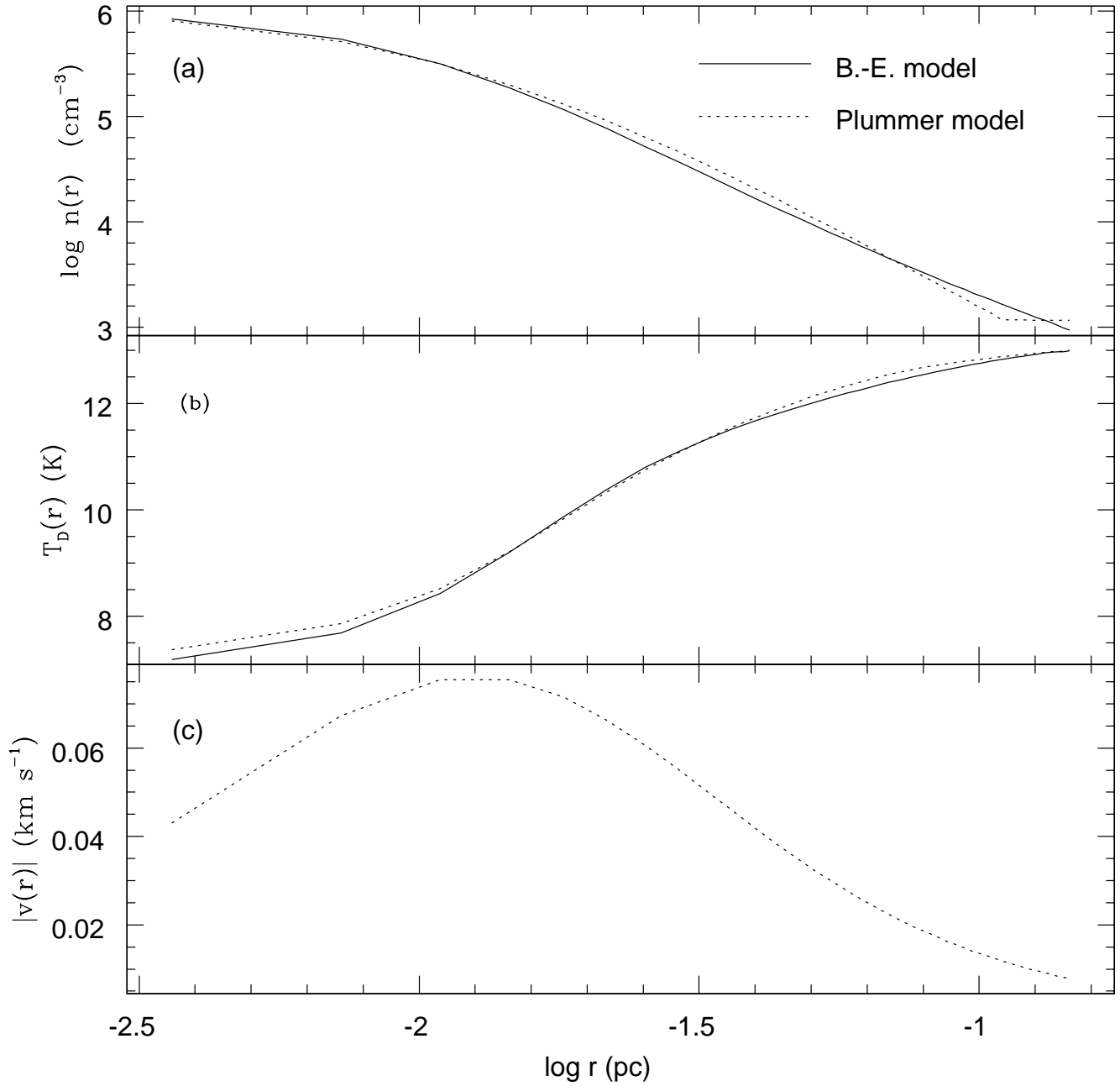


FIG. 4.— The comparison between physical parameters of the Bonnor-Ebert model and the Plummer-like model: (a) the density distribution, (b) the temperature distribution, and (c) the velocity distribution. In the density structure of Plummer-like model, we forced the lower limit of density to be 10^3 cm^{-3} .

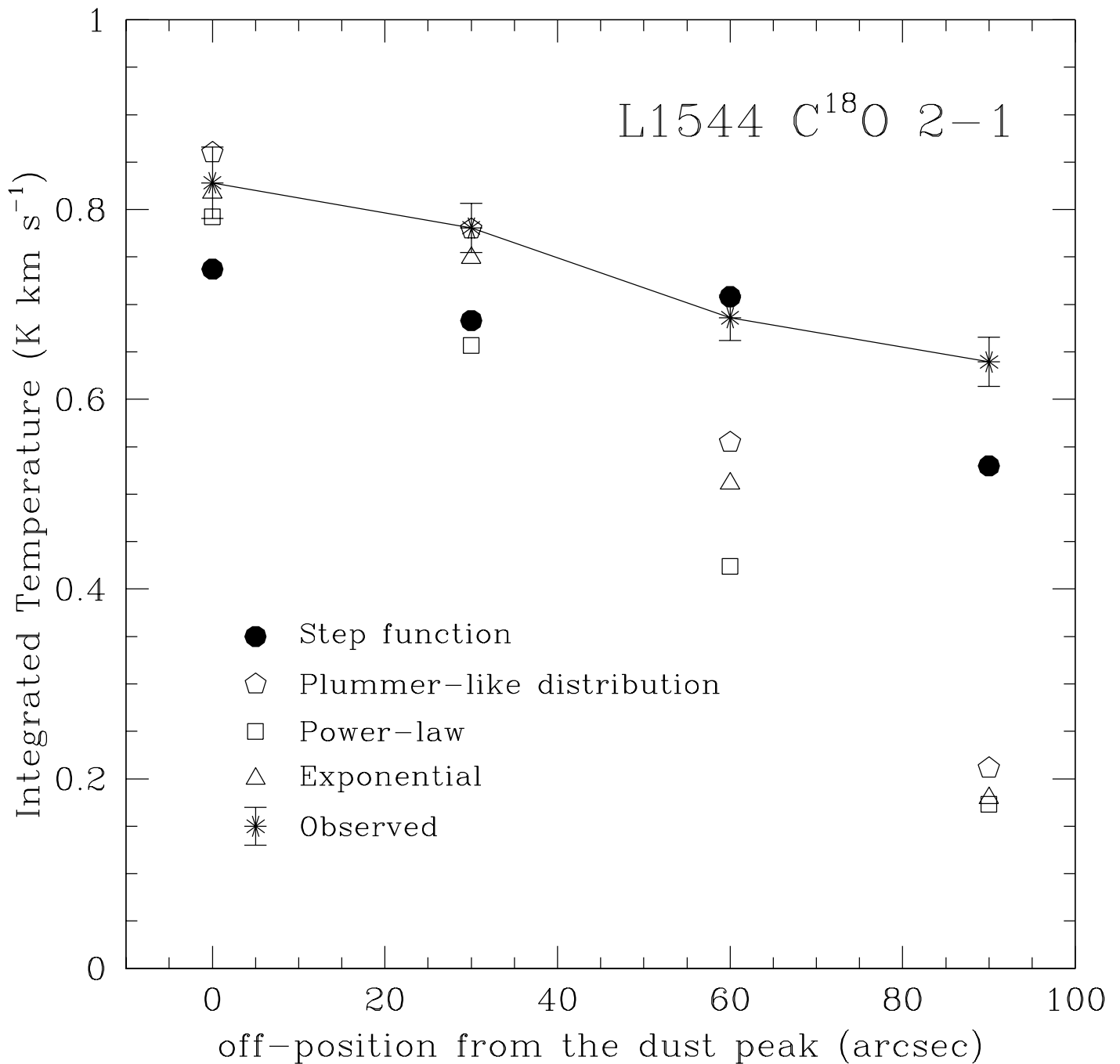


FIG. 5.— The comparison of different functional forms of depletion (Table 6). The integrated interval of velocity is from 6.5 to 8 km s⁻¹. The step function fits best the distribution of the observed integrated temperatures. The line profiles of modeling the step function is shown in Figure 7.a. The integrated temperatures of the model of the step function are smaller than the observed ones because the model does not fit the high velocity wing parts that increase the integrated temperatures in the observed lines.

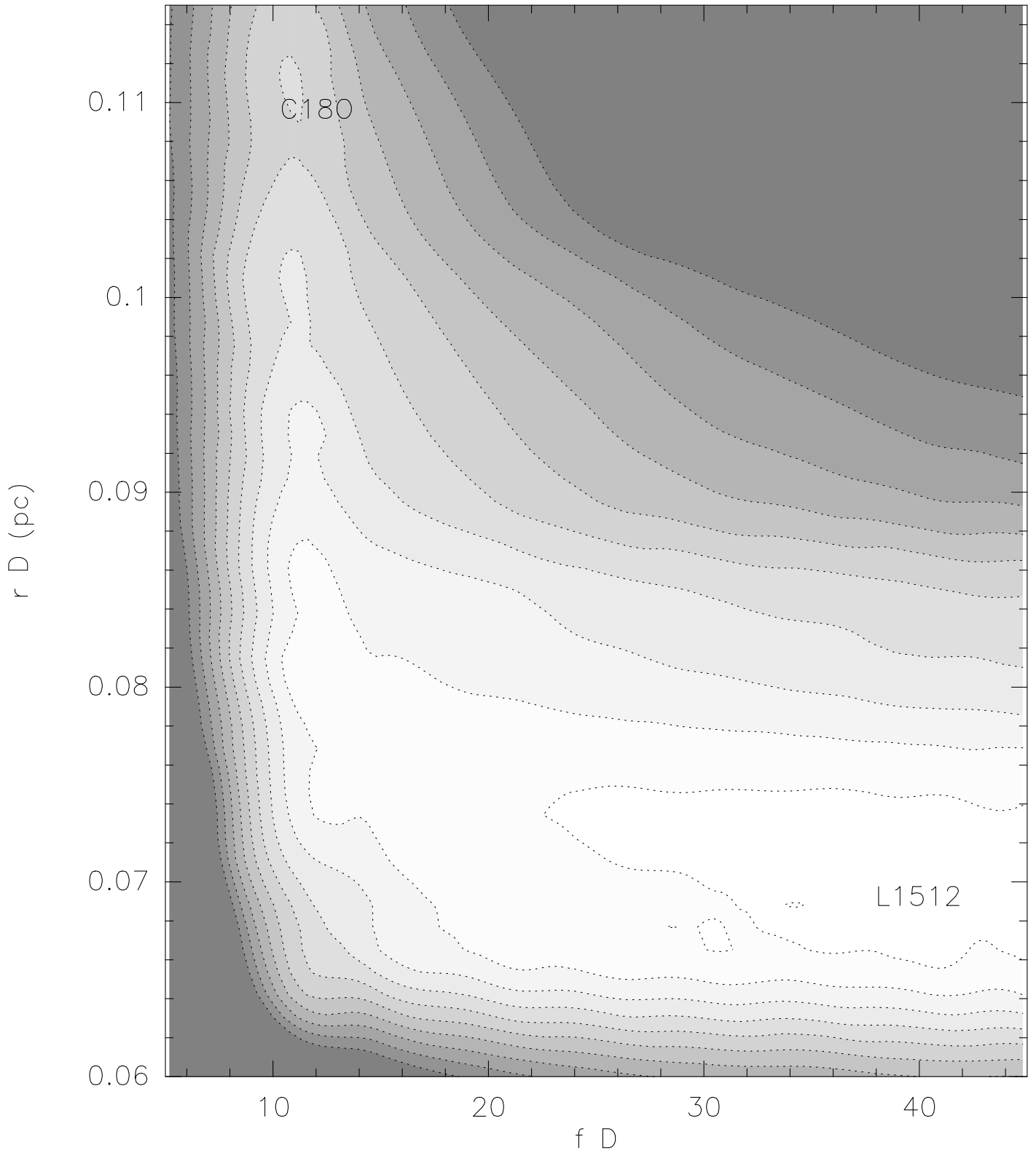


FIG. 6.A.— The distribution of the reduced χ^2 of models that have different r_D and f_D in $C^{18}O$ 2-1 and 3-2 toward L1512. The contour levels are from 5 to 95 increasing by the interval of 10. The χ^2 has been calculated by weighting the difference between the modeled and observed integrated temperatures with the errors in the integrated temperatures of the observed lines.

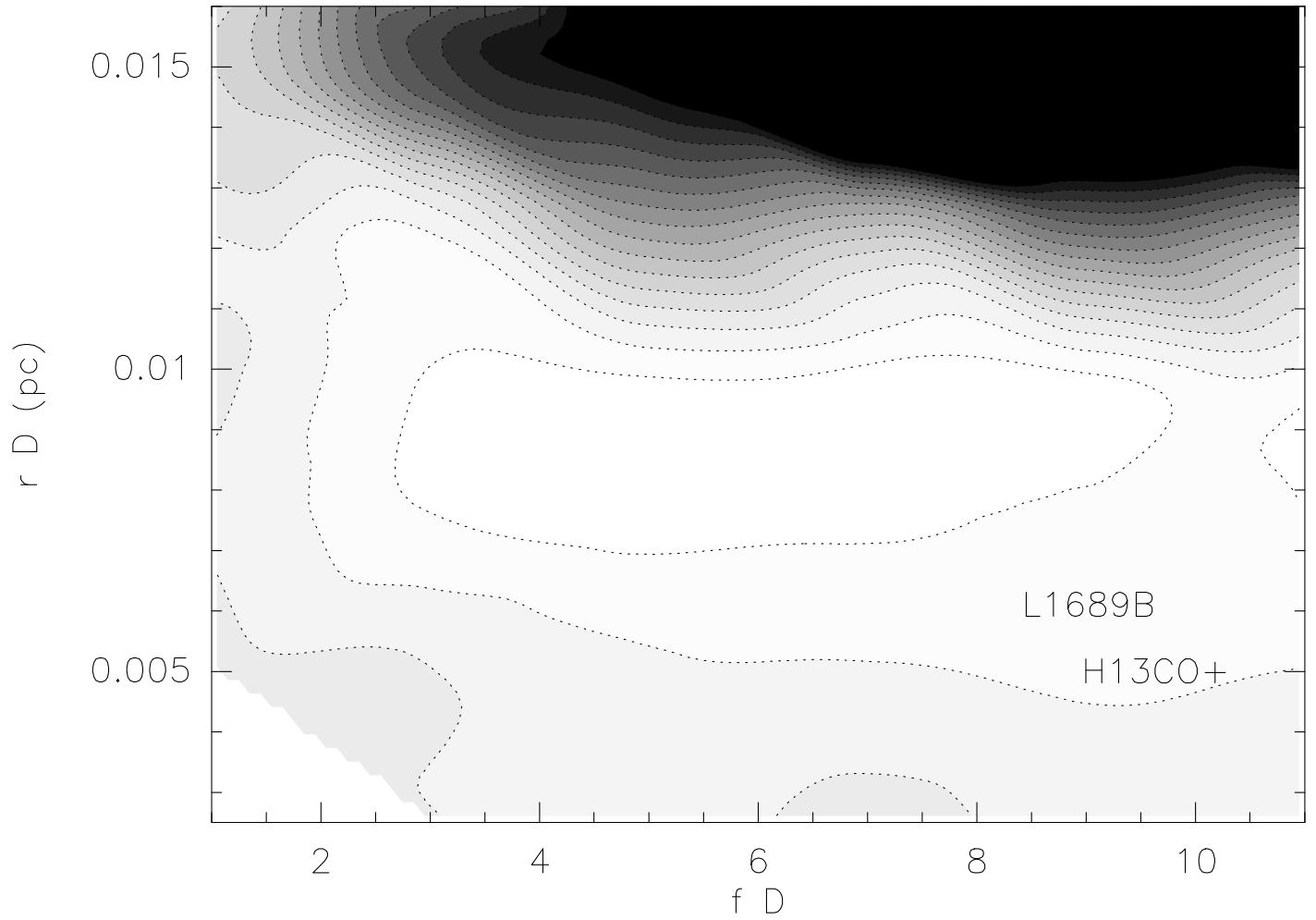


FIG. 6.B.— The distribution of the reduced χ^2 of models that have different r_D and f_D in H^{13}CO^+ 1-0 and 3-2 toward L1689B. The contour levels are from 3 to 33 increasing by the interval of 2.

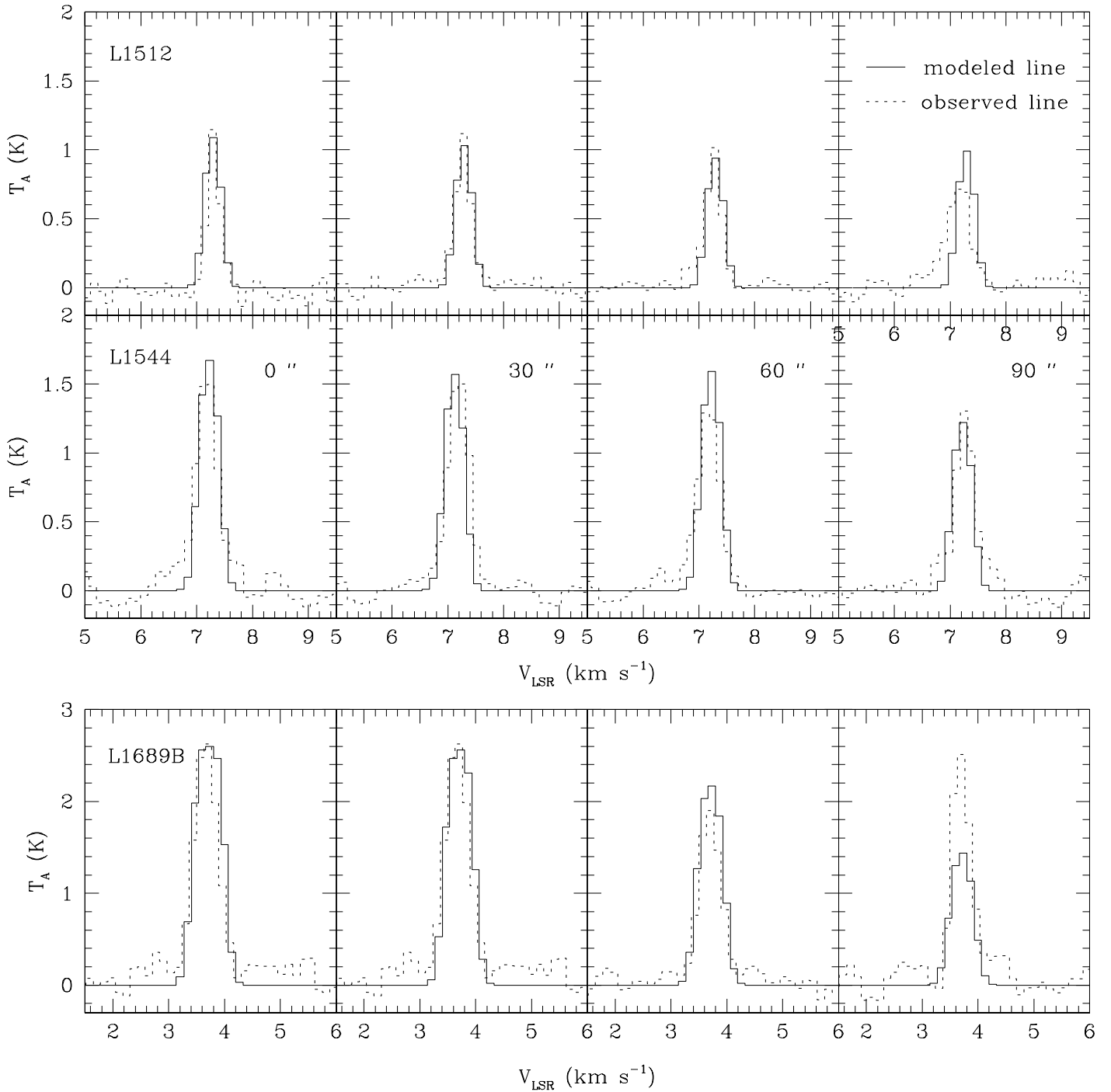


FIG. 7.A.— The results of MC modeling in $\text{C}^{18}\text{O } J = 2 - 1$. $\text{C}^{18}\text{O } J = 2 - 1$ and $J = 3 - 2$ lines have been modeled simultaneously, and we chose the abundance structure that fitted both of the lines. In each panel, the solid line and the dashed line indicate the modeled and the observed line profiles, respectively. The arcseconds marked in the middle panels represent the angular distance from the dust peak of each core.

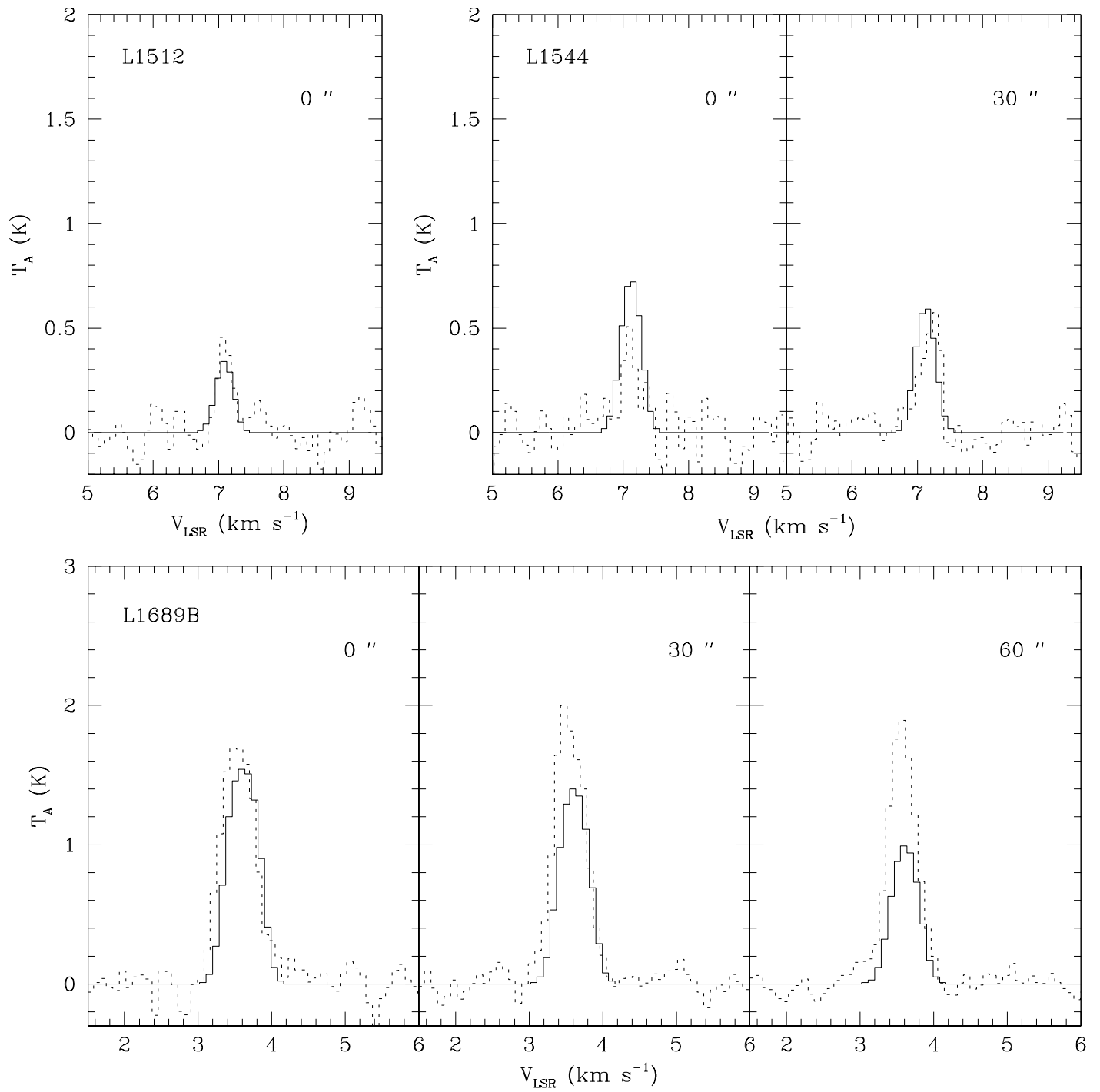


FIG. 7.B.— The results of MC modeling in $C^{18}O$ $J=3-2$.

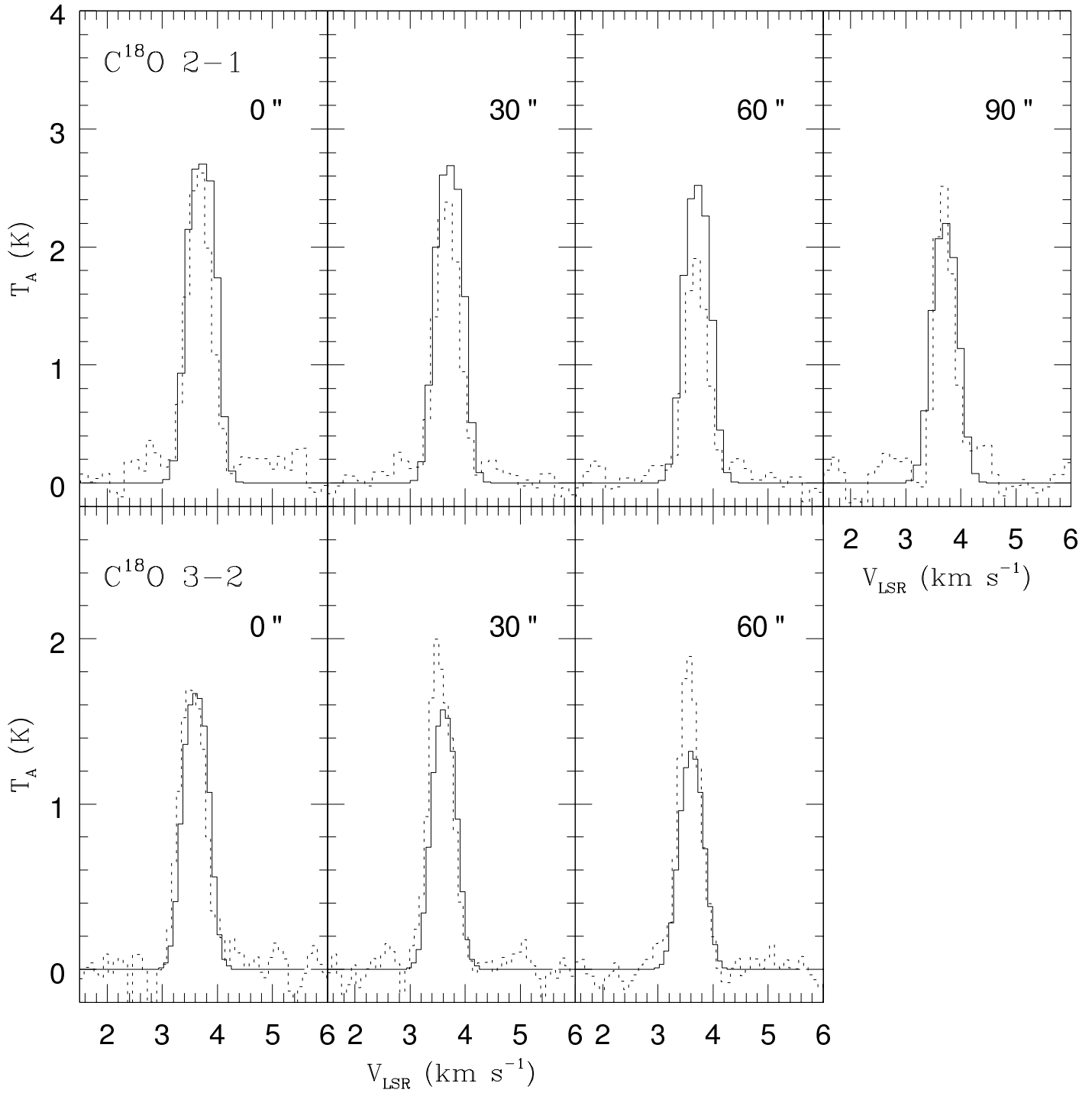


FIG. 7.c.— The results of MC modeling of L1689B in C^{18}O lines including a warm envelope.

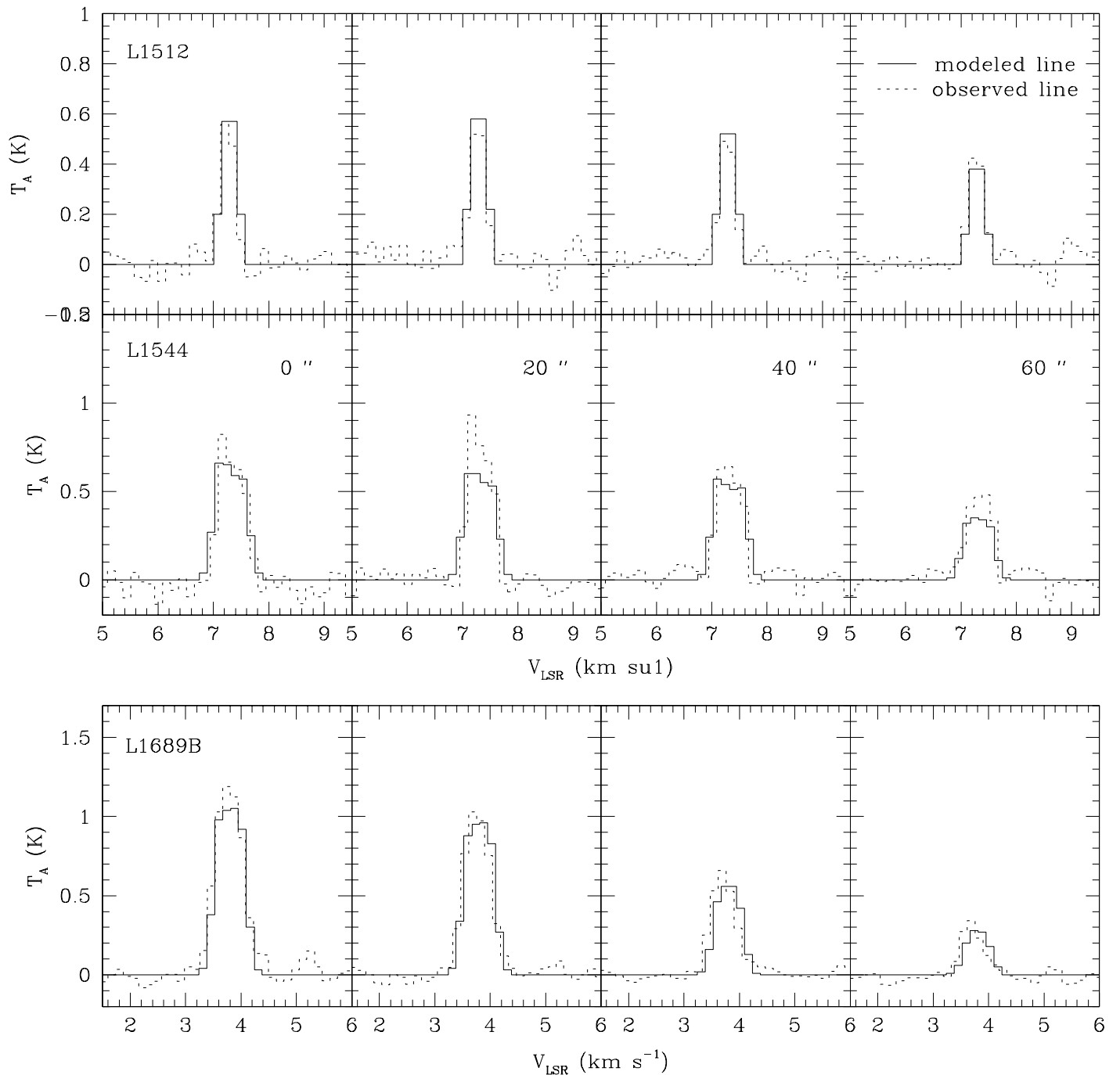


FIG. 8.A.— The results of MC modeling in H^{13}CO^+ $J = 1 - 0$. H^{13}CO^+ $J = 1 - 0$ and $J = 3 - 2$ lines have been modeled simultaneously, and we chose the abundance structure that fitted both of the lines. In order to model these line profiles, in L1512 and L1689B, we used the density and temperature profiles given by Bonnor-Ebert dust models (Evans et al. 2001), but we calculated the structures of density and temperature in L1544 combining the empirical dynamics model of Whitworth and Ward-Thompson (2001) and dust radiative transfer code.

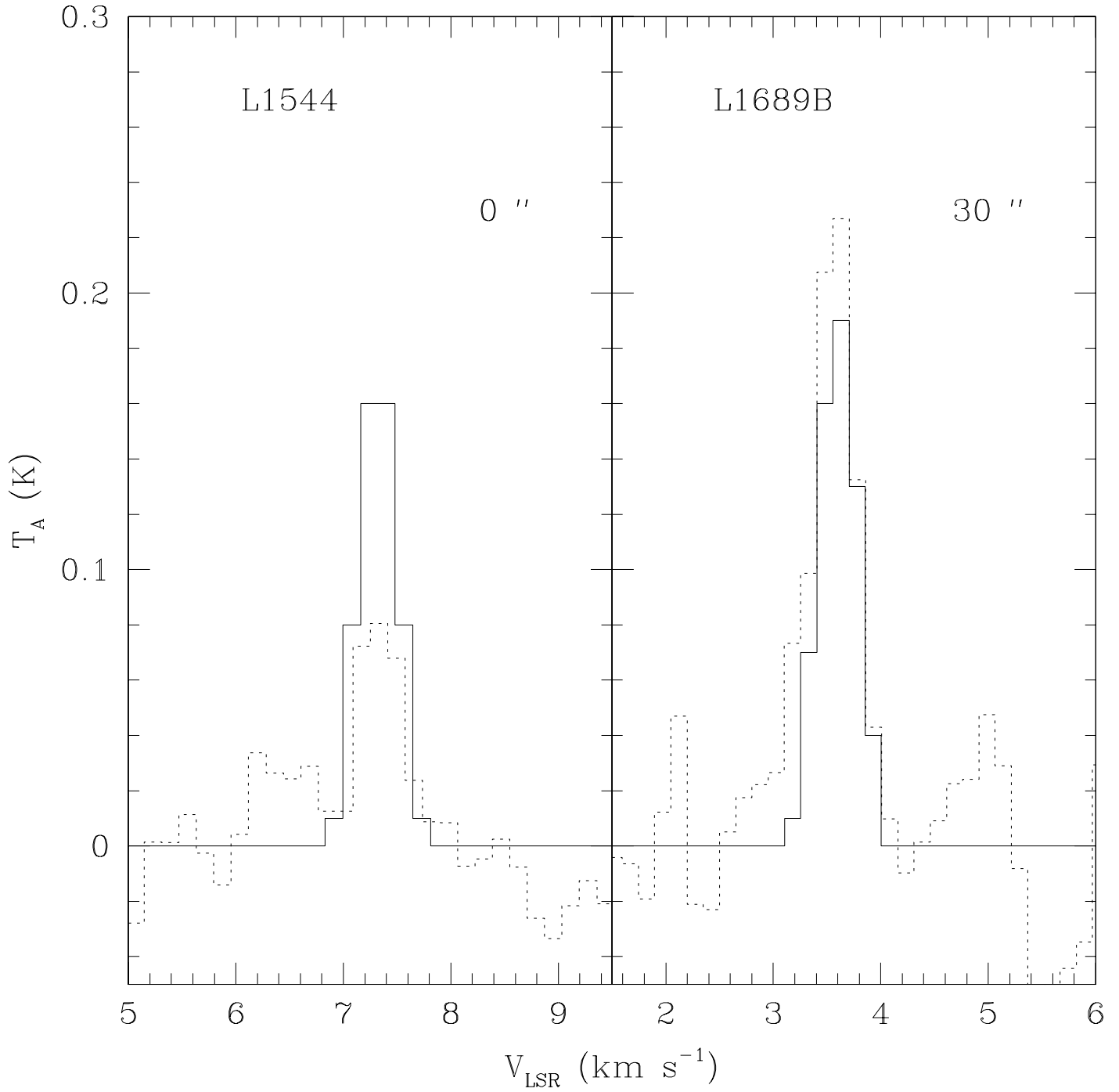


FIG. 8.B.— The results of MC modeling in H^{13}CO^+ $J=3-2$.

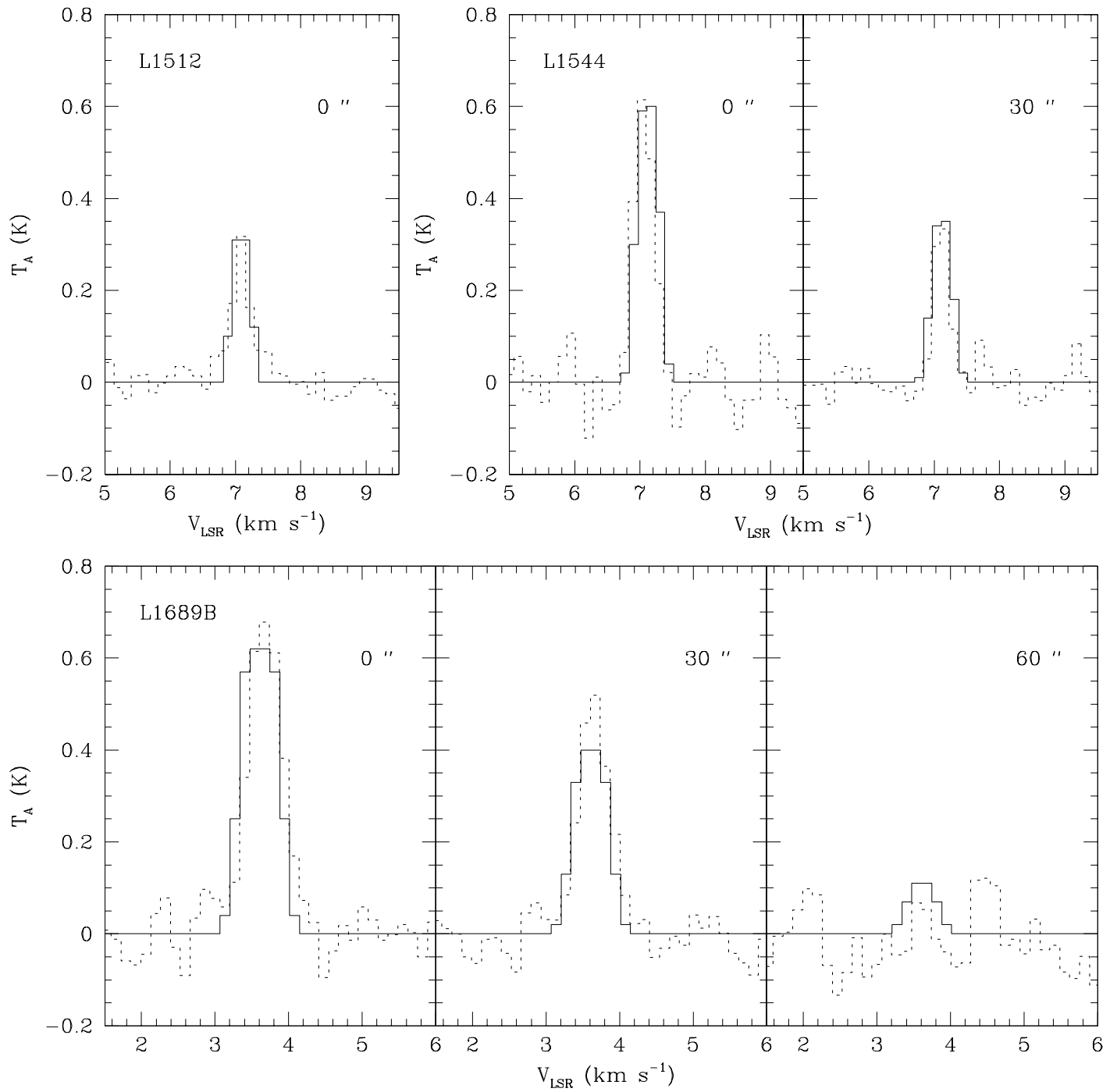


FIG. 9.— The results of MC modeling in DCO⁺ J = 3 – 2 line.

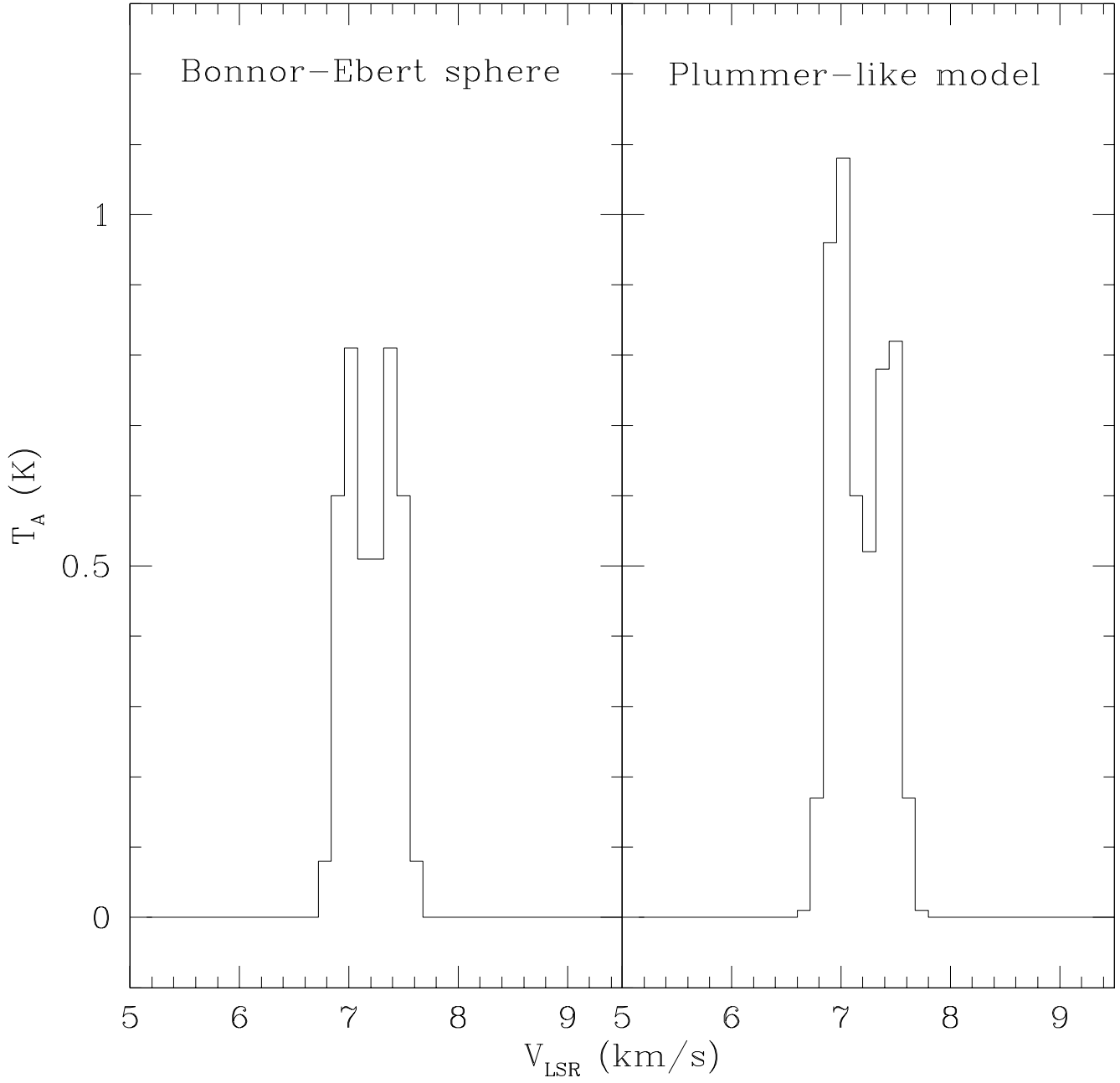


FIG. 10.— The comparison of MC modeling in HCO^+ $J = 3 - 2$ line of L1544 for two different physical models: Bonnor-Ebert sphere and Plummer-like model (see Figure 4). Both have the same abundance structure, but only the Plummer-like model, with an infall velocity structure, produces the blue asymmetry shown in observed line profiles.

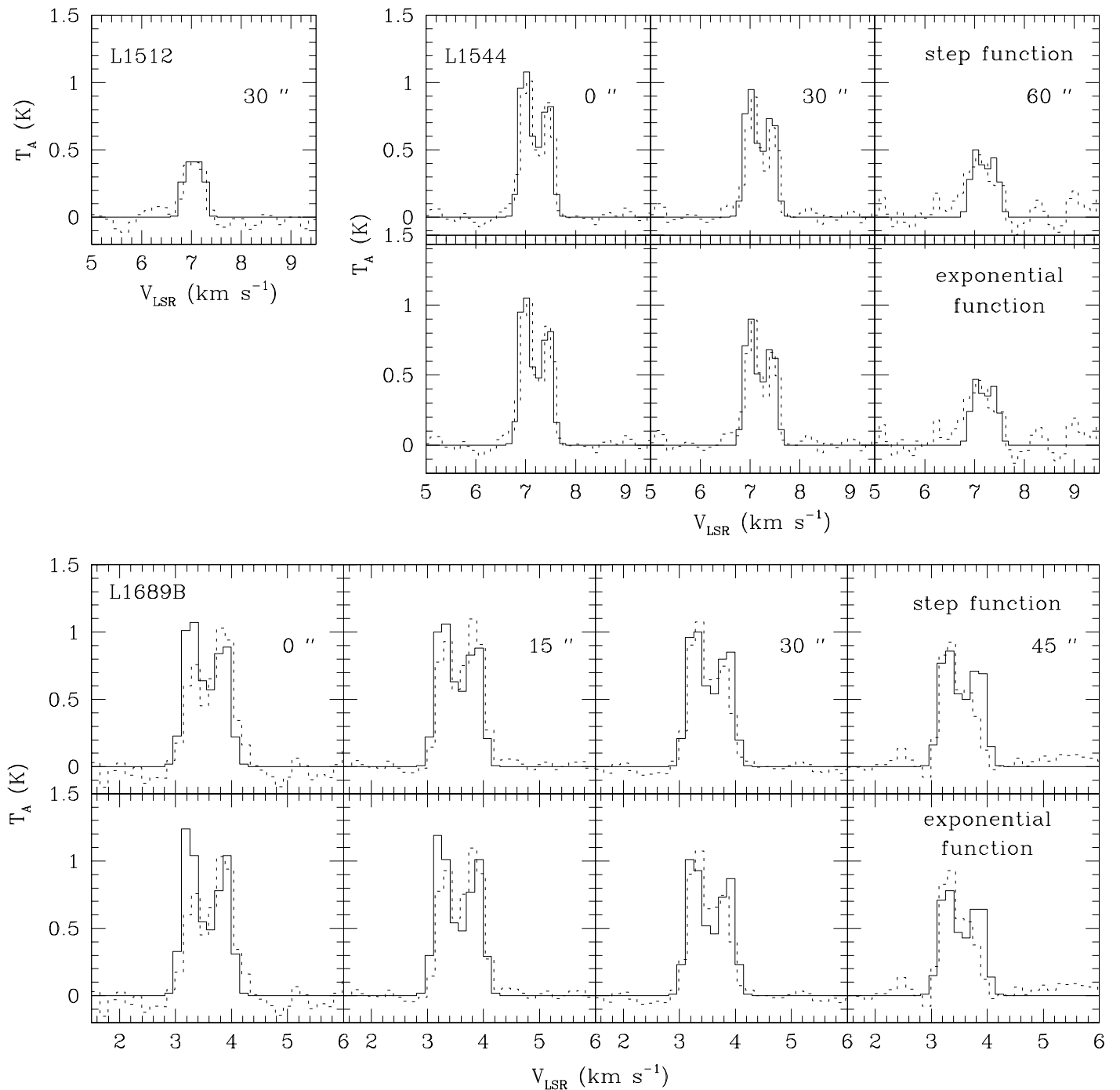


FIG. 11.— The results of MC modeling in HCO^+ $J = 3 - 2$ line. In L1544 and L1689B, the upper and the lower panels show the results by the step function and the exponential function of HCO^+ abundance, respectively. In L1512, we modeled the line profile using a constant abundance.

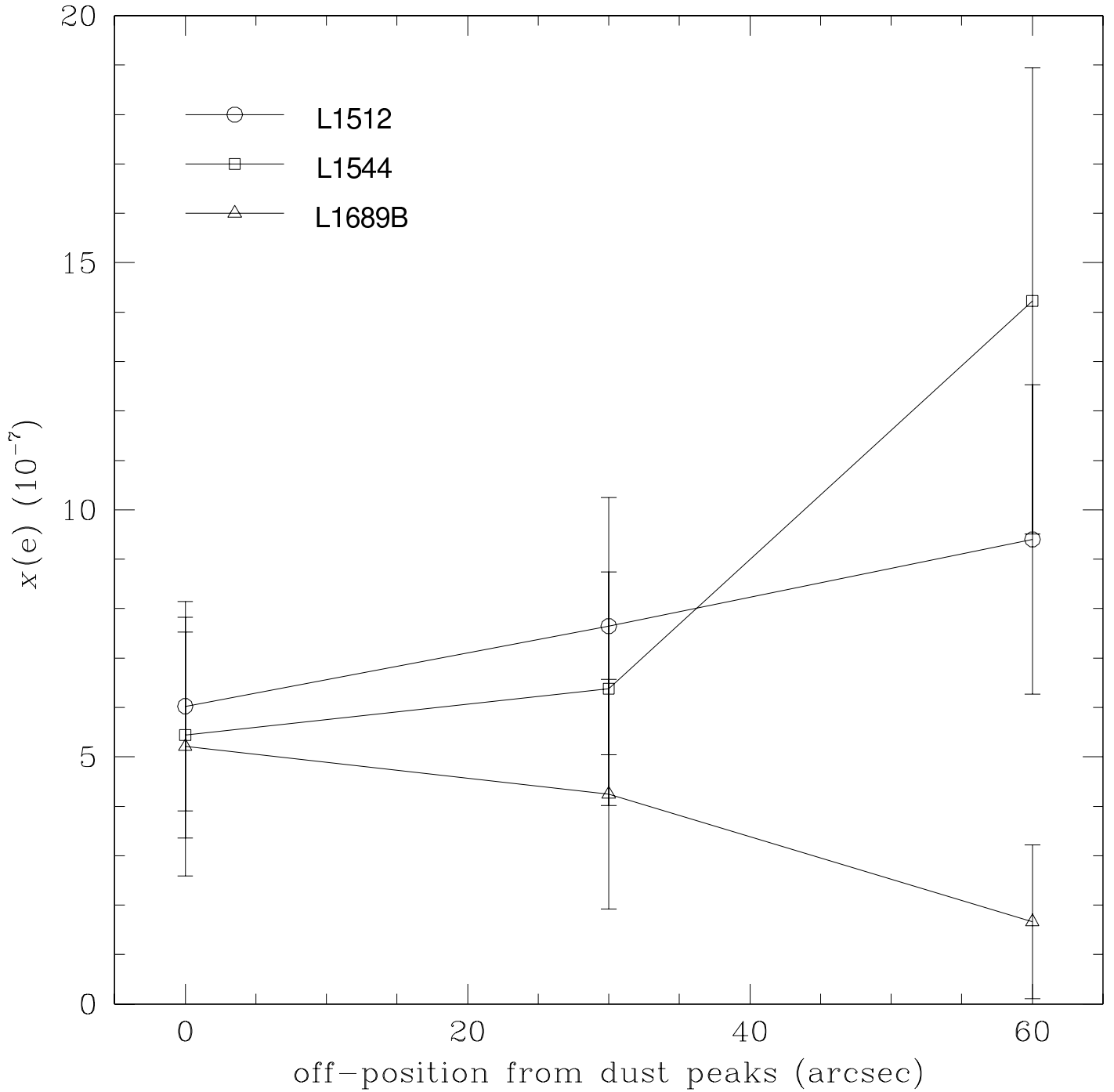


FIG. 12.— The ionization fractions in three PPCs. The error bars represent the amount of uncertainty in the ionization fraction when the ratio of $\text{DCO}^+/\text{HCO}^+$ and the depletion fraction of CO molecule changes up to 30 % of the calculated values in each point.

TABLE 1
List of sources

Name	R.A. (1950.0) hh mm ss	Dec. (1950.0) ° ' "	V_{LSR} km s ⁻¹	distance pc	offset of dust peak arcsec
L1512	05 00 54.4	32 39 37	7.09	140	(-19, -26)
L1544	05 01 13.1	25 06 36	7.12	140	(-1, 4)
L1689B	16 31 47.0	-24 57 22	3.61	125	(-1, -12)

TABLE 2
List of observed lines

Molecule	Transition	Frequency MHz	Beam Width arcsec	Velocity Resolution km s ⁻¹	η_{mb}^d L1512/L1544/L1689B
C ¹⁷ O	J = 2 - 1 ^a	224714.385	33	0.17	0.65/0.65/0.80
C ¹⁸ O	J = 2 - 1 ^a	219560.357	34	0.15	0.69/0.66/0.60
	J = 3 - 2 ^a	329330.507	26	0.10	0.59/0.59/0.63
HCO ⁺	J = 3 - 2 ^{a,c}	267557.620	26	0.15	0.49/0.66/0.65
H ¹³ CO ⁺	J = 1 - 0 ^b	86754.330	18	0.14	0.49/0.49/0.49
	J = 3 - 2 ^{a,c}	260255.617	26	0.16	none/0.49/0.65
DCO ⁺	J = 3 - 2 ^a	216112.605	35	0.15	0.65/0.69/0.60
CCS	N _J = 4 ₃ - 3 ₂ ^b	45379.033	37	0.27	0.77/0.77/0.77
N ₂ H ⁺	J = 1 - 0 ^b	93173.809	17	0.13	0.50/0.50/0.50

^aobserved with CSO 10.4 m telescope

^bobserved with Nobeyama 45 m telescope

^cGregersen and Evans, 2000

^d $\eta_{mb} \equiv T_A^*/T_R^*$, where T_R^* is the radiation temperature, and $T_R = T_R^*$ only if a source fills the beam (Kutner and Ulich 1981).

TABLE 3
Parameters for molecules

Isotope	Rotational constant B (MHz)	Dipole moment μ (Debye)	Abundance $X (= n_i/n_{H_2})$
C ¹⁸ O	54891.423	0.11079	4.8×10^{-7}
C ¹⁷ O	56179.982	0.11034	1.5×10^{-7}

TABLE 4
OPTICAL DEPTH OF C¹⁷O J = 2 - 1 LINE AT CENTER POSITION

Source	Total optical depth
L1512	0.10 (± 2.17)
L1544	1.03 (± 0.42)
L1689B	0.79 (± 0.24)

TABLE 5
DEPLETION FACTOR OF CO MOLECULE AT CENTER POSITION

Source	$N(\text{H}_2)_{\text{S850}}/N(\text{H}_2)_{\text{C17O}^{\text{a}}}$
L1512	11
L1544	9
L1689B	2

^aWe have corrected for the optical depth effect to calculate the column density.

TABLE 6
THE χ^2 IN MODELING THE C^{18}O 2–1 LINES OF L1544 BY THE DIFFERENT FUNCTIONAL FORMS OF DEPLETION

Function	X	χ^2
Step	X_0^{a} ($r > 0.045$ pc) $X_0/25$ ($r < 0.045$ pc)	10
Plummer-like	$X_0 \left[\frac{r}{\sqrt{r^2 + (0.05)^2}} \right]^2$	76
Power-law	$X_0 \left(\frac{r}{0.15} \right)^1$	117
Exponential	$X_0 \exp\left(-\frac{0.04}{r}\right)$	93

$$^{\text{a}}X_0 = 4.82 \times 10^{-7}$$

TABLE 7
THE PARAMETERS OF BEST-FIT MODELS IN C^{18}O LINES

Source	X_0^{a}	r_D^{a} pc	f_D^{a}	$V_{\text{microturbulence}}$ km s^{-1}
L1512	4.82×10^{-7}	0.075	25	0.15
L1544	4.82×10^{-7}	0.045	25	0.17
L1689B ^b	4.82×10^{-7}	0.03	3	0.20

^a $X = X_0$ ($r \geq r_D$) and $X = X_0/f_D$ ($r < r_D$) where X_0 is undepleted abundance, r_D is the radius within which a molecule is depleted, and f_D is the fraction of depletion.

^bWe could not find a good model to fit all line profiles in all observed positions in L1689B.

TABLE 8
THE PARAMETERS OF BEST-FIT MODELS IN H^{13}CO^+ LINES

Source	X_0	r_D pc	f_D	$V_{\text{microturbulence}}$ km s^{-1}
L1512	3.0×10^{-10}	0.021	25	0.07
L1544	5.0×10^{-10}	0.026	20	0.20
L1689B	2.2×10^{-10}	0.012	5	0.20

TABLE 9
THE PARAMETERS OF BEST-FIT MODELS IN DCO⁺ LINES

Source	X_0	r_D pc	f_D	$V_{\text{microturbulence}}$ km s ⁻¹
L1512	2.8×10^{-10}			0.09
L1544	3.5×10^{-10}	0.022	3	0.12
L1689B	3.5×10^{-10}	0.011	4	0.20

TABLE 10
THE PARAMETERS OF BEST-FIT MODELS IN HCO⁺ LINES

Source	step function		exponential function ^a		$V_{\text{microturbulence}}$ km s ⁻¹	
	X_0	r_D pc	f_D	X_0		r_D pc
L1512	1.0×10^{-9}				0.1	
L1544	3.0×10^{-9}	0.028	10	6.0×10^{-9}	0.04	0.15
L1689B	3.2×10^{-9}	0.023	15	6.5×10^{-9}	0.03	0.20

^a $X = X_0 \exp(-\frac{r_D}{r})$

TABLE 11
THE RESULTS OF THIS STUDY

	L1512	L1544	L1689B
Degree of central condensation	Young	Evolved	Evolved
Chemical evolution (depletion of molecules)	Evolved	Evolved	Young
Timescale	$\tau_{che} \ll \tau_{dyn}$	$\tau_{che} \approx \tau_{dyn}$	$\tau_{che} \gg \tau_{dyn}$
Dynamical state	Stable (?)	AD (?)	Free-fall (?)